Magyar Agrár- és Élettudományi Egyetem

MONITORING WATER QUALITY APPLYING THE SPECTRAL PROPERTIES OF LIGHT

Theses of the doctoral dissertation

András Barczi

DOI: 10.54598/003700

Gödöllő

2023

The name of the

doctoral school: Doctoral School in Engineering

field of science: Engineering

president: Prof. Dr. Kalácska Gábor
university professor, DSc
Hungarian University of Agriculture and Life Sciences
Technical Institute

consultant: Dr. Géczi Gábor
habilitated assistant professor, PhD
Hungarian University of Agriculture and Life Sciences
Institute of Environmental Sciences

. . . .

Approval of president Approval of consultant

Table of contents

1. Background and objectives of the work

„The key question is what we are looking at in relation to what.”
(Dr. Csizmadia Béla)

For humans, bodies of water are not only a source of health, food, income and energy, important transport routes and recreational places: water is essential to our lives. The existence, condition and use of water, especially fresh water, is one of the most important factors in our lives. Since water is not available in unlimited quantities, if we are to ensure that everyone has access to clean drinking water in the future and that rivers and lakes remain a key part of our landscape and our lives, we must make efforts to protect and improve the status of surface and groundwater. The importance of rivers, streams, lakes and groundwater is not only natural, but also economic, as they provide opportunities for income generation and expenditure, and therefore their conservation is a vital and timely task.

However, water use comes at a price: urbanisation, population growth and increasing human activity have led to an increase in the amount of wastewater generated - and therefore the amount of wastewater that needs to be treated. The quantity and quality of domestic wastewater is constantly changing with human lifestyles. Contaminated water contains harmful substances, including disease-causing bacteria, viruses, organic wastes, inorganic substances (salts, acids, heavy metals), inorganic plant nutrients (nitrates, phosphates), organic compounds (oils, detergents, pesticides). Water pollution makes water partially or completely unfit for human use and damages natural aquatic life processes. Continuous sampling of water supply systems and detailed

analytical and microbiological testing to detect water pollution are therefore a priority to ensure water quality. In the case of environmental contamination, testing should be extended to surface water and soil around the water source, allowing the path of the contamination to be traced. In order to ensure that our water use is sustainable and thus provide sufficient quantity and quality of drinking water for future generations, potential water pollution must be eliminated at source (Csősz, 2019).

The basic rules of water management in Hungary are laid down in Act LVII of 1995 on water management, as amended several times. It provides the basis for the general system of state and municipal environmental protection activities, while at the same time defining the structure of the environmental management system and the responsibility of society as a whole for the protection of the environment through the responsibility of individuals.

1.1. Timeliness of the topic

Sustainable water management requires efforts from both industrial and domestic water users. Adaptation to the impacts of global climate change is also necessary in terms of water management and water use (Takács, 2019). Water pollution in our time takes many forms, and although the scale and form of these forms of pollution vary considerably from continent to continent, country to country, region to region, there is one common link: water itself, our lifeblood. Water is not just a hydration medium, it is an excellent hygiene compound, it has huge economic and energy potential (fisheries, shipping, hydroelectric power) and, although its buffer capacity is huge, it is not infinite. It takes a different approach to clean up ocean pollution or to slow down, halt or reverse a process of eutrophication that is underway. As 50-80% of the

oxygen we need to breathe is produced by algae in the oceans that connect the continents of our planet (Chapman, 2013; Witman, 2017), countries without a coastline or ocean coastline cannot escape pollution efforts, and the responsibility is much more extensive. It is also a fact that the neglect or expropriation of water bodies can be a source of international conflict.

The development of instruments to control artificial treatment technologies has meant the development and intensification of different ways of removing nutrients, the development and intensification of small-scale wastewater treatment, and the more effective retention of toxic pollutants that are difficult to degrade or hazardous to receiving waters. All technologies rely to a greater or lesser extent on biological processes to 'naturalise' pollutants. Surface water monitoring in developed countries is typically carried out using rapid chemical tests, which require considerable care both in their storage and in their application. Unfortunately, for reasons that are not well understood, rapid tests are rarely disposed of in hazardous waste storage after use, and even after their expiry date, with the result that the data obtained from their measurements are distorted.

Sewage treatment plants are monitored using probes. It is also an unfortunate fact that the use of uncalibrated probes in a neglected state is often observed, with the direct consequence that the efficiency of the treatment plant is reduced due to the use of biased data. However, this situation is not necessarily due to neglect or lack of demand: they are not in a position to buy new or more probes to keep operating costs down. In developing countries, the situation is much worse: population growth and industrialisation are outpacing the ability to build the new infrastructure needed to treat the associated wastewater. Even today, wastewater is sometimes discharged into

the watercourse itself; even if the water supply comes from a borehole or is piped, the wastewater system is not necessarily well developed, i.e. there is no collection system. However, the treatment of wastewater not only increases the volume, but also makes the water supply much more predictable, as the generation of wastewater is largely independent of the weather. In Africa, South and South East Asia, the pollution of the seas and oceans is very high, but without sufficient capital injection, the situation is getting worse every year, as our world thinking and political views become more and more bipolar. This is to the detriment of the environment: developing and developed countries blame each other for the environmental pressures caused, and in the heat of the debate, there is a failure to find solutions (Barczi and Géczi, 2018).

In the future, much more attention will have to be paid to reducing pollutants entering water at an early stage, otherwise effective wastewater treatment can no longer be guaranteed. Although EU countries are relatively problem-free in collecting and treating wastewater, 80% of the world's countries do not even have wastewater treatment plants, so water pollution remains a daily problem (Kümmerer et al., 2018).

Wastewater treatment is a topical environmental issue, as legislation is forcing industrial polluters to adopt new techniques not only to recover their valuable products, but also to reduce their emissions. On this basis, the extent of wastewater treatment required is influenced by the conditions at the receiving site, the volume of wastewater to be treated, the amount of pollutants that can be discharged to the receiving site with the treated wastewater, economic considerations and treatment limits set by water protection legislation in each country (Postel, 2000). Preference should be given, on the basis of environmental considerations, to treatment processes that are themselves

associated with low environmental impact and minimal waste product (Appels et al, 2008).

It is also relevant to the present situation that, by using the sewage network almost universally, it is a quick and cheap way to obtain representative health information and the resulting data can support and help in making appropriate decisions (Pandics et al., 2021), as was the case during the Covid-19 epidemic.

As early as 1986, Smalley (2005) pointed out in his university lectures that water was the second of the top ten global problems. He argued that until the issues and challenges related to water and water management are resolved, the other nine global problems (in order: energy, water, food access, pollution, poverty, war and terrorism, disease and epidemics, maintenance of democratic values, population issues) will remain unsolved.

The use of remote sensing in agriculture and environmental protection is also gaining ground. Fields used for agricultural crop production, as well as living water and wastewater, can be monitored. Therefore, not only satellite data collection, but also data collection by aircraft, drones, etc., plays an important role in both precision agriculture and environmental protection. The combination of continuous and highly accurate positioning (GPS/GNSS), Geographic Information System (GIS) support and remote sensing allows, for example, the automation of agricultural work and the continuous monitoring of vegetation and environmental damage. It can also be used to map detected anomalies and damage. Together, these can increase agricultural production, improve environmental protection and, not least, make all these activities more cost-effective.

1.2. Purpose

In the literature part of my dissertation, I reviewed academic books, journal articles and internet studies, supplemented my existing experience with previous doctoral theses and conference publications, and reviewed relevant legislation in the field. Consequently, I have included a separate chapter on water quality, light and remote sensing in the literature. In the section on water quality, I will explore the classic and recent relevant scientific findings and research results related to living waters, wastewater and indicator organisms and algae in water. For the chapter on light, I look beyond the physical properties of light to colour theory, colour perception and digital imaging technology. In the chapter on remote sensing, I discuss its role in environmental protection. In the Materials and Methods unit, I describe in detail the instruments used for sampling measurements and the measurement sites. In the empirical part of my research, I present the results and the conclusions drawn from them. The new scientific results are presented in a separate chapter.

As I have found that developments in the field of wastewater treatment are rather slow, my aim was to develop a water quality determination method based on the spectral properties of light to assist in the maintenance and/or rehabilitation of living waters and the operation of wastewater treatment plants. In the implementation of this method, I want to keep in mind accuracy, ease of use, fast response time and low operating costs. The basic aim of my research is therefore to provide scientific results to facilitate water quality determination and to accelerate monitoring technologies and possible interventions.

The development of the monitoring system will begin with the development of data and mathematical equations. I focused primarily on the loads from the agricultural sector and wastewater treatment, and therefore chose to look at the phosphate (PO_4) and total nitrogen (TN) content of the water. I also aimed to extend the possibility of colour monitoring: we need to know the potential limits and confounding factors of this extension. I have assumed that the use of image-monitoring tools for environmental purposes has not yet reached its peak, and that technological advances will open up new possibilities in this area, so I have carried out the empirical part of the research with the image-monitoring tools described in detail below.

Overall, I examined the indicator organisms living in the water, the colouration and physical/chemical properties of several water bodies. Taking into account the differences between the imaging devices, the remote sensing capabilities, the interfering and interfering factors in remote sensing, I have constructed a model that can provide efficient information for the monitoring system to be developed, not to mention quickly and quite cost-effectively.

Research related questions:

Q1: Is there a correlation between the colour of the water and the chemical parameters (TN, PO_4) that influence its quality?

Q2: How accurately can the instantaneous quality of water be determined by colour analysis?

Q3: What interferences can occur during low-altitude remote sensing?

Q4: What level of uncertainty can occur with CMOS sensors in colour analysis applications?

2. Material and method

In this chapter, I describe the sampling and measurement tools, image capture devices and methods used for data analysis and descriptive statistics. I describe the calibration procedures and then describe the experimental sites where the measurements were taken. Finally, I will present a flowchart showing how my investigations were carried out, what was tested against what, and in which areas.

2.1. NIX Color Pro, NIX Color Sensor Pro

At the start of the research series, I planned to use only cameras with CMOS sensors, but after the first few measurements it turned out that natural light variations, weather, and the time of measurement all distorted my results, so I needed a tool that could eliminate these distractions and give accurate, unbiased numerical data on the measured colour. Of course, I did not give up my basic plan to develop a method that was accessible to everyone, but I did not want to replace CMOS sensors with colour measurement, but to write down a mathematical equation for the difference by comparison, so that the method could be applied to additional camera types.

I used the NIX COLOR PRO and NIX COLOR SENSOR PRO, a brilliantly shaped device measuring just 8 x 8 x 8 centimetres from the Canadian developer Nix Sensor Ltd. The product is described as a device developed for food quality control, dye testing and dye calibration (Figure 1).

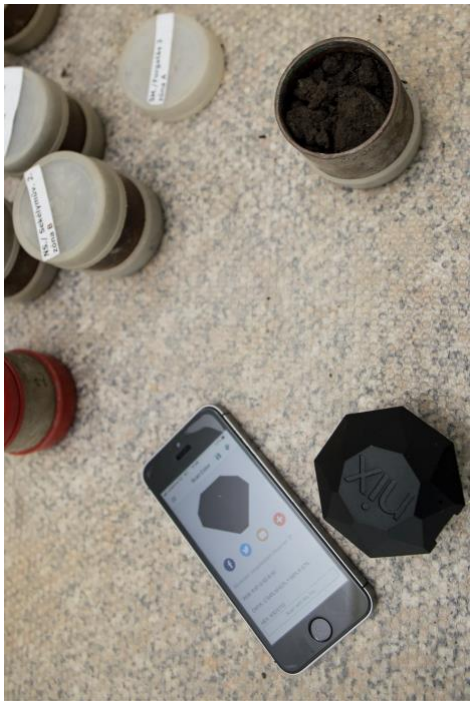

Figure 1: NIX Color Pro during a soil colour test.
Source: own image

The device is small, mobile and easy to store. It gives accurate values even after multiple measurements, so the data set it generates is considered reliable. In terms of its operation, the device creates a small enclosed space above the area to be measured, other light sources from the side are not a concern, as I have verified by measurements; I placed the colorimeter on a color map and then placed light sources with different Kelvin values, first further away and then closer to the colorimeter, while it did not move out of place.

From 2020 onwards, I used the NIX COLOR SENSOR PRO for colour measurements, which, although similar in appearance to the previous version, is much more advanced. The colour measurement itself is, according to the company, more accurate and the software can take reference values, so that the data can be plotted not only in a table but also immediately in, for example, a LAB coordinate system. This allows, for example, polygon values to be

analysed for a number of replicate measurements, and later the figures for the visually determined polygons can be analysed individually. I used the two tools in parallel, so I could be sure of the accuracy of the colour measurement.

When measuring with the NIX COLOR PRO or the NIX COLOR SENSOR PRO, color accuracy was assured, but when measuring liquids, the company suggested that I compensate 35 or 50% in color saturation (for white backgrounds), or if the background is not white, to take the background color and compensate downwards 35 or 50%.

2.2. DJI AIR S2

The installation of a surface camera system is often inadequate for measuring bodies of water; parts of a concave pond or even the anaerobic biological reactor of a sewage treatment plant are often not visible on the images. This has not been a problem for the Environmental Engineering Laboratory's reactors with a water surface area of approximately $1m^2$, but larger surface areas can cause problems.

In 2018, I passed my drone pilot exam and in June 2021 I purchased my own DJI AIR S2 (Figure 2), which was considered the best recording drone on the market in 2021.

Figure 2: DJI Air S2 drón.
Source: https://dji-official-fe.djicdn.com/cms/uploads/eead2358fecb94ceb86d412f4ca4b67d.png

It has a range of up to 18.5 km and a flight altitude of up to five km above sea level, but Hungarian and EU law allows these aircraft to climb to a maximum altitude of 120 m to avoid endangering air traffic. The minimum flight/descent altitude is 0.5 m (measured by lower range sensors), during which the aircraft will engage in an automatic landing manoeuvre. It can stay airborne for 25-30 minutes on a single battery, depending on wind conditions, has a top speed of 70 km/h and the stabilisation system can maintain altitude and heading up to a gust of 10.7 m/s. The LiPo 3S battery has a power of 3500 mAh and a consumption of 42.42 Wh. The vehicle weighs 595 g (battery included) and measures 180 mm x 253 mm x 77 mm when ready to fly. The camera is mounted on a three-axis gimbal stabilizer, tiltable between 90 and -24 degrees, with a vibration excursion of less than 0.01°. The 1" CMOS sensor is capable of capturing 20 MP (5472×3648; for 3:2 aspect ratio) still images at 2.4 μm pixel size in jpeg or RAW (*.DNG) format. The lens is 88° (wide-angle, full-frame equivalent 22 mm), with a fixed aperture of f/2.8. It has a 10-bit colour depth (I chose 8-bit mode for my tests), so colours are accurate, making dynamic separation easy. In continuous mode, two to three *.DNG images per second can be captured.

2.3. Additional imaging tools

2.3.1. SJCAM 4000

When choosing the cameras, the sensitivity of the sensor and the colour depth of the captured image were decisive, but it was also important that the camera could automatically take a series of repeated photos even under water, so that after image processing was completed, the colour changes could be seen in

fast time-dimension through a time-lapse video. The SJCAM 4000 camera (Figure 3) captures 12 MP (4032*3024 - 4:3 aspect ratio) images with a pixel size of 2.2 µm on a 1/3" sensor of the AR0330 type, which are compressed into *.jpeg format with 10-bit colour depth (for the tests I converted to 8-bit colour depth).

Figure 3: SJCAM4000.
Source: https://www.sjcammagyarorszag.hu/img/41446/ep-sjcam-sj4000-wifi/ep-sjcam-sj4000-wifi.jpg

The cameras' 900 mAh battery has a maximum usage time of around three to four hours for continuous shooting, but only 70-90 minutes for movie recording, which is not enough for our measurements. By modifying the waterproof case, I connected the camera to an external source via a Micro-USB port, so that recording could continue until the MicroSD card was full. The camera can accept a MicroSD card with up to 64GB of storage, and was able to record for approximately five days without stopping, which means 6800-7200 images depending on image size.

2.3.2. Canon 6D

This Digital Single-Lens Reflex (DSLR) camera features a full-frame (24 mm x 36 mm) CMOS sensor capable of capturing 20.2 MP pixels at 5472 x 3648 pixels with a pixel size of 6.54 µm. Image capture modes include manual, remote and time-lapse recording. The camera also has built-in GPS, so

repositioning was not a problem. I used a Canon EF 16-35mm f/2.8L II USM zoom lens on the frame for the measurements. The horizontal angle of view of the lens can be varied between 98º-54º. Colour depth of field is 8-bit.

2.3.3. iPhone SE

have chosen this device because it has a similar type of sensor (although the name is different) to the SJCam4000 described in section 2.3.1, so the only difference here is the lens elements and the image processing software. The sensor type is a backlit Sony Exmor RS IMX315, capable of capturing 12.2 MP (4032 x 3024) images with a pixel size of 1.22 μm and 8-bit colour depth. The lens elements are equipped with a built-in IR filter and have a fixed aperture of f/2.8.

2.3.4. Xiaomi Mi 8

The Xiaomi Mi 8 smartphone sensor type is not disclosed by the manufacturer. The sensor itself is capable of capturing 12 MP (4000 x 3000) images with a pixel size of 1.4 μm and a colour depth of 8-bit. The fixed aperture of the lens elements is f/2.2.

2.4. Additional measuring instruments

2.4.1. Exact iDip

The chemical and physical parameters were measured with an eXact iDip photometer owned by the former Szent István University of Civil, Plant and Environmental Engineering. The instrument is mainly used for the

measurement of pools, aquariums, ponds, drinking water, but I also made measurements during the image acquisition at a wastewater treatment plant (together with the accurate measurement data from the wastewater treatment plant in Gödöllő), to verify the accuracy of the instrument. The photometer was used to test the following chemical parameters:

- pH,
- calcium (Ca),
- copper (Cu),
- nitrite (NO_2),
- nitrate (NO_4)
- total nitrogen (TN),
- total phosphate ion (PO_4).

During the measurements in the bioreactor, pH, nitrite, nitrate and phosphate were measured and recorded every time, copper and calcium only once a week.

The photometer can be controlled via an app written on a smart device. The device has a four ml reservoir, where the sample is loaded. During the measurement, the photometer is covered so that the measurement is not affected by any external light source. Inside the container, depending on the model, there is a light source with a wavelength of 525 nm and a propagation distance of 11 mm. The device also has an LCD display that shows the test name and result, but this data is also available via an app. eXact iDip runs on 4 AAA batteries and communicates with smart devices via Bluetooth. As well as test strips for each parameter being measured, some of which are shown in Figure 4.

Figure 4: Test strips for the eXact iDip instrument.

Source: own image

After loading the sample, I selected the parameter I wanted to test via the app, and I also selected the test strip for that parameter. After pressing the READ button, a 20-second countdown starts, during which the test strip is soaked in the sample. When this time has elapsed, the light stopper cap is placed on the instrument and the measurement is taken.

The measurements are performed in triplicate and the average of the measured results is recorded in an Excel spreadsheet. If the standard deviation was greater than 10%, another measurement was taken and the data with the highest standard deviation was replaced by the newly obtained measurement result.

2.4.2. Measurement of meteorological parameters

During measurements 3.1 and 3.2 temperature and during measurement 3.4 wind speed was measured and recorded. The temperature was measured with

an EBI 300 (EBRO, Germany) temperature data logger. The EBI 300 has a measuring range between -30C° and +60C° degrees (accuracy ±0.5 °C), can store a total of 40,000 values, and the measuring time interval (and readout) can be set via USB port using Ebro® online configurator.

Wind speed measurements were performed with a FVAD 15 (Ahlborn, Germany) wing wheel wind speed meter. The measuring range of the wind speed meter is between 0.2 m/s and 40m/s with a resolution of 0.01 m/s. This measuring instrument was connected to an ALMEMO-2490-4 (Ahlborn, Germany) data logger via an ALMEMO ZA9909-AK1U connector.

2.5. Accredited laboratories

After the identification of the measurement series described in sections 3.1 and 3.2, the validation was carried out several times not with a parameter measured by myself, but with a test performed in an accredited laboratory. The water analysis measurements performed by KVI-Plusz Ltd. (Eurofins KVI-Plusz Ltd., Budapest, Szállító u. 6, 1211) covered the following parameters:

- Total dissolved solids
- Total dissolved salt
- Chemical oxygen demand (COD)
- Phosphate (PO_4)
- Total nitrogen (TN)
- pH
- Free Chlorine (DPD-1)
- E. Coli count
- Coccus count

In addition, the identification and validation results of the series of measurements described in section 3.3 are also the results of laboratory tests provided by the Gödöllő wastewater treatment plant.

2.6. Description of the sampling and measurement processes

When I was sampling, it was important to me to interfere with the environment in the smallest way possible and always work with the right amount of sample. I kept safety and health regulations in mind. No protected plants or animals were harmed during the sampling.

2.6.1. Collection and processing of water samples

I collected the water samples in 0.2 l PET bottles, after rinsing three times with water on the spot, trying to sample the deeper layers of water that were within reach of my hands. I returned the samples to the Environmental Technology Laboratory, where I sampled the droplets with a dropper after shaking for 30 seconds, and then used a colorimeter to record the color data of the droplets when placed on white tiles. I then immediately wiped the tile and repeated this three times.

I tried to use as few PET bottles as possible for the measurements, bearing in mind the environmental impact of PET.

2.6.2. Storage and disposal of samples

There was no need to store samples because sample processing and data retrieval were instantaneous. For the water samples, I used the sewer system,

since occasionally less than 0.5 l of sample was used, which did not contain high concentrations of components that were hazardous to the environment.

2.7. Software and methods applied in the measurements

2.7.1. Adobe Photoshop, Adobe Lightroom

For image processing I used Adobe Photoshop, and for multiple repetitive images Adobe Lightroom.

After importing the images, I started processing in these programs. White balance (WB) adjustment was done in one of the programs, correction of exposure values of the images based on the shooting histogram.

The images were then exported, keeping the original uncompressed format of the images: *.DNG for the drone, *.CR2 for the handheld camera, and *.tiff for the handheld camera.

Depending on the test, the previously exported images were re-imported in PS, not per separate file, but per layer, so that averaging could be performed much easier, using a written PS-Script, averaging could be applied to all image layers in the file.

When averaging, I used a polygon to take the target area, zooming into the images for the most accurate selection possible. I applied pixel-based averaging to the polygonal area; this script analyses all pixels in the target area and then averages them by colour band (R, G, B) and displays the resulting colour (Figure 5).

Figure 5: The left image shows a photograph of the lake, and the right image shows the average colour fill after the lake has been circled with polygons.

Source:own image

2.7.2. Microsoft Excel

I used Microsoft Excel to record and evaluate the measurement results. The significant functions I used were averaging "=Average()", moving average, expanding average, standard deviation "=STDEV()", minimum "=MIN()" and maximum search "=MAX", correlation search "=CORREL()" and linear regression fit "=LINEST()". For RGB visualisation and analysis, I most often used bar charts or dot plots, while the CieLAB visualisation was done in a dot plot coordinate system.

Also in Excel, I did the trendline fitting, where I chose the linear trendline, wrote out the equation of the line and the value of the R-squared.

I also did the rounding here, because in RGB coding natural numbers can appear (0-255), in CIELAB coding the L value (0-100) and A-B values (-128-+128) can take a fractional value up to two tenths of a digit due to the 8-bit color depth sensors. These values are dimensionless values and have no units of measurement.

To check the identification of mathematical models and to evaluate the validation, I used the relative error (h_C) over the measurement range (Géczi et al., 2019; Kicsiny, 2018, 2017; Kline, 1953; Székely et al., 2021).

$$hc = \frac{\overline{H_c}}{C_{max\ measured} - C_{min\ measured}}\ [\%] \tag{1}$$

where:

- $\overline{\boldsymbol{H_C}}$ – the absolute error of the modelled concentration,
- $\mathbf{C_{measured}}$ – measured concentration,
- $\mathbf{C_{mod}}$ – modelled concentration,

The mean absolute error of the modelling ($\overline{\boldsymbol{H_C}}$) is calculated as the average of the differences between the measured concentration ($C_{measured}$) values and the modelled concentration (C_{mod}) values:

$$\overline{H_c} = \frac{|C_{mémeasured\_1} - C_{mod\_1}| + |C_{measured\_2} - C_{mod\_2}| + \cdots + |C_{measured\_n} - C_{mod\_n}|}{n} \tag{2}$$

where:

- **n** – number of measurements.

2.8. Additional UAVs

or the drone measurements, I did not use only one type of drone for the assumed interference effects of the drone's self-produced air movement, but I made measurements with two additional types of aircraft.

The first machine type is the DJI Mini 2 unmanned aerial vehicle. This type of machine has a total weight of 249 g, can accelerate to 58 km/h and has a maximum altitude of 4,000 metres. It has a maximum climb speed of 5 m/s and a maximum descent speed of 3.5 m/s. Airborne endurance 27-31 minutes. I did not take any pictures with this aircraft.

The second type was the DJI Mavick Pro. This type of aircraft weighs 734 g, has an acceleration of 65 km/h and can climb to an altitude of up to 5000 m. Its time in the air is 21-24 minutes. It has a maximum climb speed of 5 m/s and a maximum descent speed of 3 m/s. I did not take any pictures with this type of aircraft.

2.9. Measuring sites

2.9.1. Parallel bioreactors

I carried out two six-month measurements in two experimental basins (called bioreactors) set up in the Environmental Engineering Laboratory of my university. The two reactors are built of the same materials and cladding, with the same piping, so they are identical. Their dimensions are 140 cm x 75 cm, giving a water surface area of 1.05 m^2, the bottom of the reactor is 50 cm from the surface, and the process water height is 35 cm, giving a process volume of 0.3675 m^3 per reactor. No technological cover was used, so the experiments

are completely outdoor. The bioreactors are located next to each other, so their environmental exposure is the same (Figure 6).

Figure 6: Bioreactors and their exposure. Source: own image

The bioreactors were operated in parallel, all measurements were performed in parallel. They are called:

1: active or experimental reactor: this is where the chemical dosing took place

2: reference or control reactor: this reactor received the same water and was exposed to the same environmental conditions, but no chemical dosing was performed.

To exclude differences in algae formation in the experimental reactors, the waters were mixed after filling, so that each series of measurements started with a homogeneous water body with similar physical and chemical parameters.

- Education pond No 4

2.9.2. Education pond No 4 of Isaszeg, Hungary

For live water measurements, I selected the rearing pond No. 4 of the Isaszeg fishing pond operated by Aranyponty Zrt. (Figure 7). The pond is approximately 50 m long, 15 m wide, east-west oriented, with an average operating depth of 120 cm and an approximate water volume of 900 m^3.

Figure 7: Breeder pond No 4 in the environment. Source: own image

The lake is connected to the Isaszeg fishing lake system, fed by the back-flowing Rakos stream, with approximately 15 m^3 of water changed every hour, so the total water change takes approximately three days. The pond receives its water from the outfall of the Gödöllő wastewater treatment plant.

2.9.3. The Gödöllő wastewater treatment plant and its anoxic reactor

In agreement with the wastewater treatment plant (Figure 8), I took 15 air samples from the anoxic reactor of the wastewater treatment plant (Figure 9). The data on the chemical processes in the reactor were provided by the

wastewater treatment plant in Gödöllő. The recording was carried out on a fixed-programmed route to exclude any deviations due to altitude, and each flight was scheduled between 11.00 and 12.00 am.

Figure 8: The Gödöllő wastewater treatment plant, with the Isaszeg lake system in the background. Source: own photo

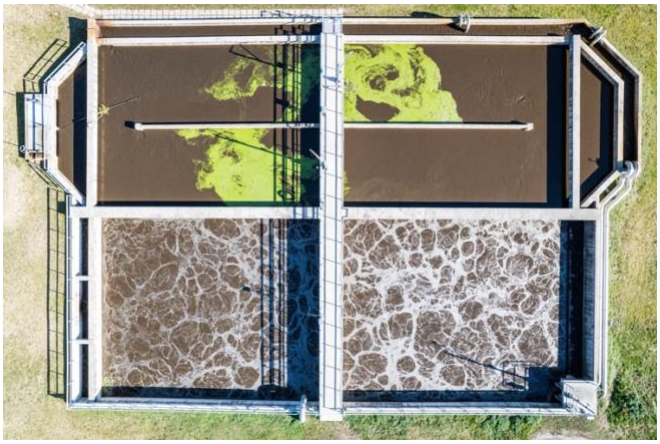

Figure 9: The anoxic (top) and aerobic (bottom) reactors of the Gödöllő wastewater treatment plant. Source: own photo

2.9.4. Additional sites used for validation

To validate the models calculated by my measurements, I carried out parallel measurements in the bioreactors described in section 2.9.1 on the one hand, and on the other hand, I carried out measurements on live water samples to see how well the measurements in the artificial environment correspond to the natural or landscape-like environment.

Validation measurements on water bodies were carried out at three sites between 2019 and 2022:

- Isaszeg Nursery Lake No 4 (2.9.2.) (2019, 2020, 2021, 2022)
- Lake Úrréti, Gödöllő (2019)
- Private bathing lake, Gödöllő (2020)

The measurements were performed in a similar way as in the bioreactors; with similar methodology and equipment, and in several cases the results were provided by the accredited laboratory of KVI-Plusz Kft. (Eurofins KVI-Plusz Kft., Budapest, Szállító u. 6, 1211).

3. Results and discussion

In the chapter Results and discussion of results, I present the evaluation of the measurements I carried out in six subsections. First, I will compare the total nitrogen concentration and water colouration in RGB colour space carried out in 2019, and then I will analyse the phosphate ion concentration and water colouration in RGB colour space carried out in 2020. For these two analyses, I have taken into account the Decree 10/2010 (VIII.18) of the VM, which sets limits, thus defining good ecological status. In the third subsection, I will analyse the anoxic reactors of the wastewater treatment plant from the point of view of water colour and phosphate ion in the reactor. In the fourth and fifth subsections, I investigate the factors that cause uncertainty in unmanned aircraft and examine whether higher altitude affects the colour of the perception. Finally, I investigate additional devices with CMOS sensors to see if 8-bit sensors can be used as a substitute for a calibrated colorimeter if the color measurement is to be used for condition determination.

3.1. Results of a correlation study of water colour and TN content

In our domestic waters, the occasional overuse of fertilisers and the occasional inadequate treatment of wastewater often cause nitrate loading, but I did not want to limit the analysis to this compound, so I measured TN (Total Nitrogen) levels. The measurements were carried out in 2019, over a period of 4 months, with 3 weekly samples, in comparative bioreactors set up in the Environmental Science Laboratory of the then Szent István University of

Mechanical Engineering. During my previous measurements I found a correlation between the total nitrogen content of water and the B band of the RGB spectral field, which was confirmed by the subsequent correlation search. The measurement series started on 23/04/2019 and ended on 09/09/2019. During this period, samples were taken three times a week (Monday, Wednesday, Friday), where each time, in addition to TN concentration, a colour measurement was performed.

In addition to TN content and colour analysis, I also measured water temperature, pH level, and occasionally bound and free chlorine, calcium and copper loading due to the use of mains water. The correlation search between temperature values and TN content and between temperature values and measured colour values did not show any correlation, so I used temperature values only as an interval in which measurements were taken and I can justify my findings for this range in the new scientific results.

The results of the correlation search for the color space and TN values are summarized in Table 1 for both bioreactors, and the visual representation of the experimental reactor is shown in Figure 11, and the focus on the B-band after the correlation search is shown in Figure 12 (experimental reactor) and Figure 13 (control reactor).

Table 1: Correlation search results between TN and colour space in both experimental reactors.

	R/TN corr	G/TN corr	B/TN corr	$R_{kontrol}/TN_{kontrol}$ corr	$G_{kontrol}/TN_{kontrol}$ corr	$B_{kontrol}/TN_{kontrol}$ corr
Correlation	0,43	0,05	**0,85**	0,18	0,24	**0,87**

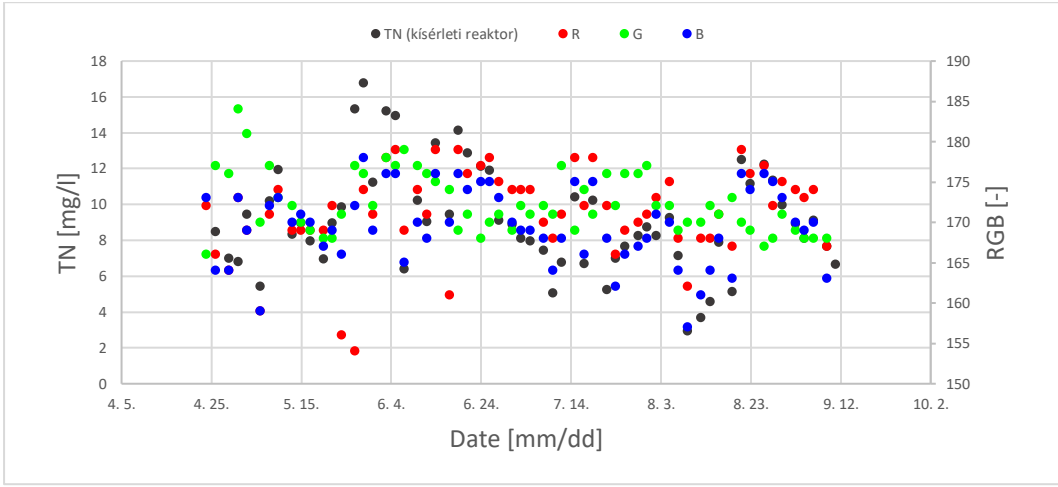

Figure 11: Display of TN concentration and RGB colour space in the experimental reactor.

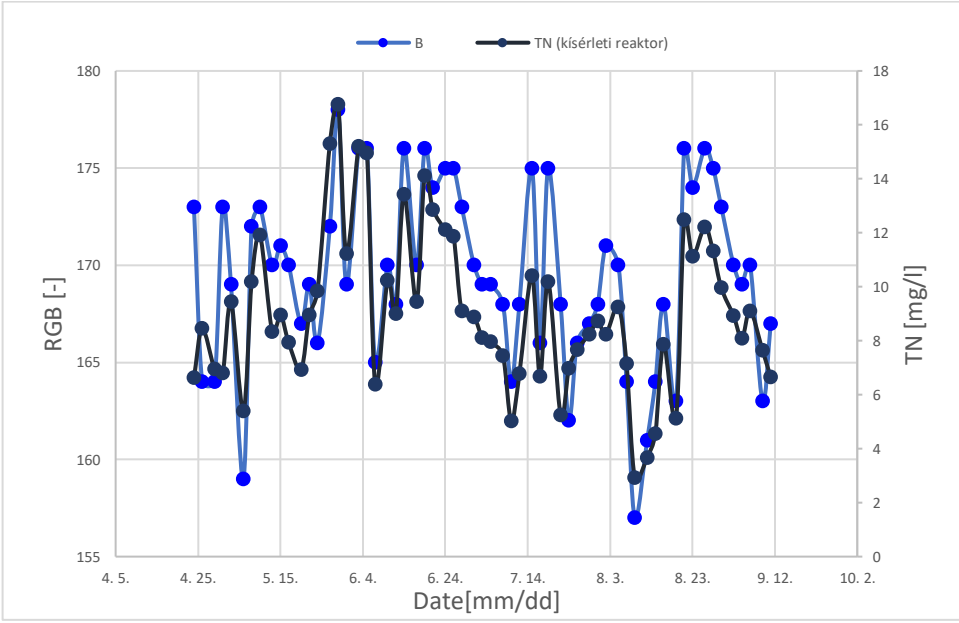

Figure 12: TN concentration and RGB colour space B-band display in the experimental reactor

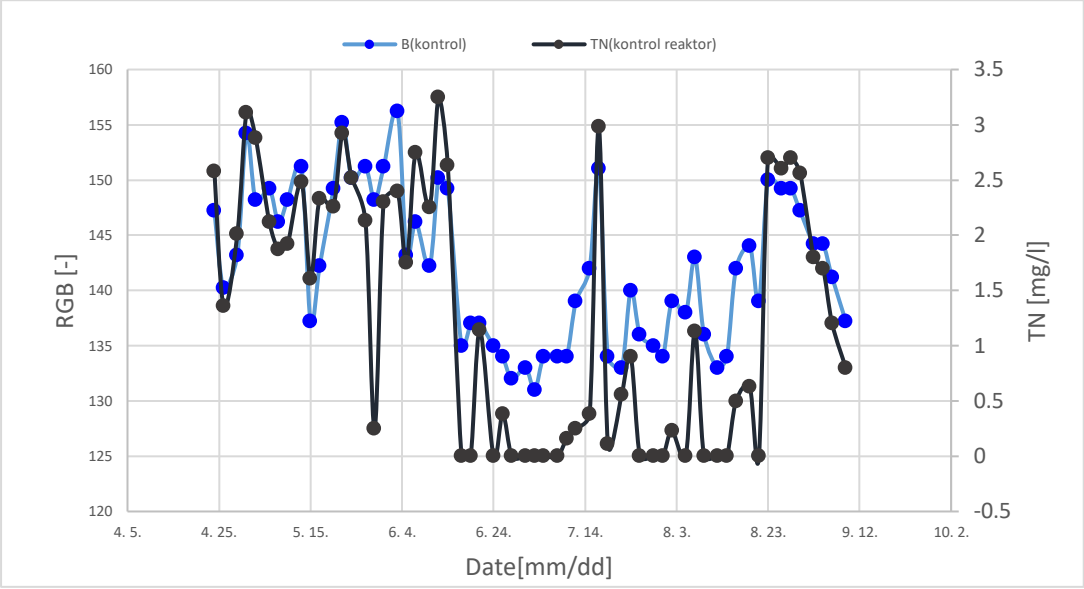

Figure 13: B-band display of TN concentration and RGB color space in the control reactor.

Plotting the measured TN values as a function of the B-band, after a linear straight line fit, the experimental reactor R^2 is 0.71 and the control reactor R2 is 0.76. Due to the overlap between the measured TN values of the two reactors, I finally plotted the measured values of the two reactors in the same coordinate system, so the identification was not 60 but 120 points.

The R^2 value of the resulting linear equation is strengthened to 0.87 (Figure 14). The identification equation is:

$$TN = 0{,}2823B - 38{,}794$$
$$R^2 = 0{,}8755 \qquad (3)$$

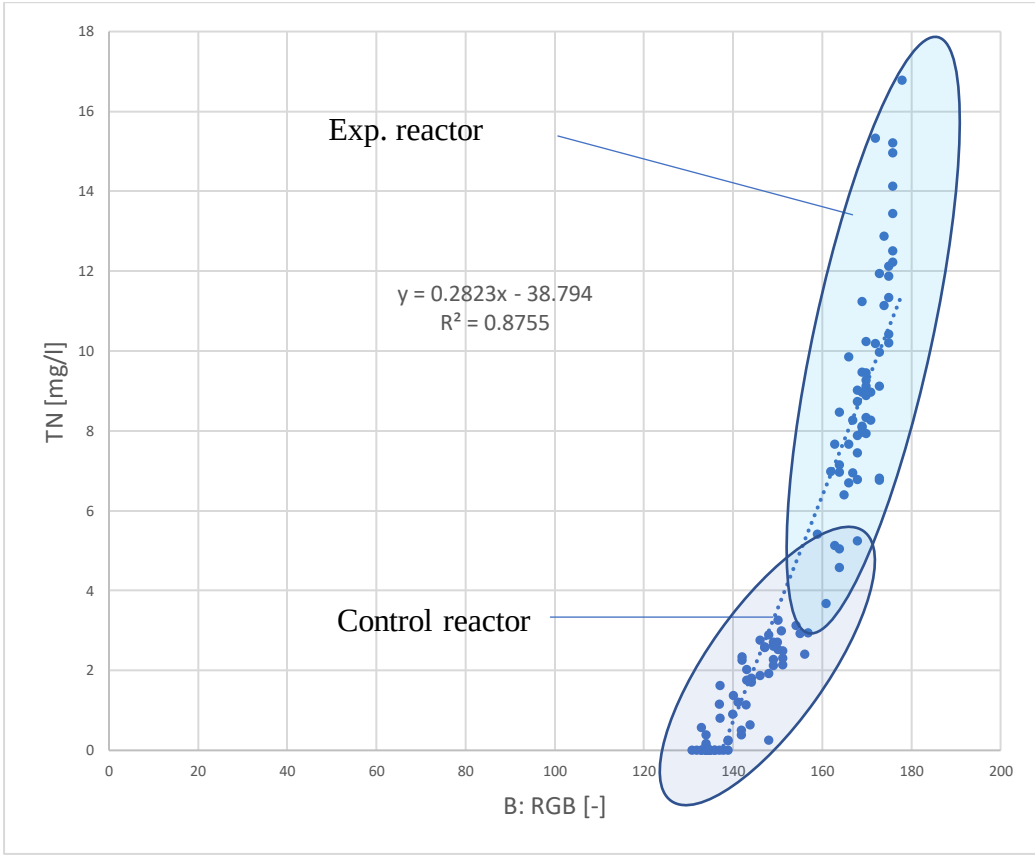

Figure 14: Measured TN values of both reactors as a function of the B band of the RGB colour space for identification.

Using the calculated equation, I plotted the measured TN values as a function of the calculated TN values, and then validated with additional sets of measurements (53 members in total, 5 sets of measurements, 4 of which were live water bodies and one artificial pool) and plotted them graphically to visually verify the success of the validation (15 Figure). For both identification and validation, I performed a search for absolute error (H_C) followed by a relative error analysis (h_C) per measurement range. The calculated linear correlation per measurement range relative error result is h_C= 6%.

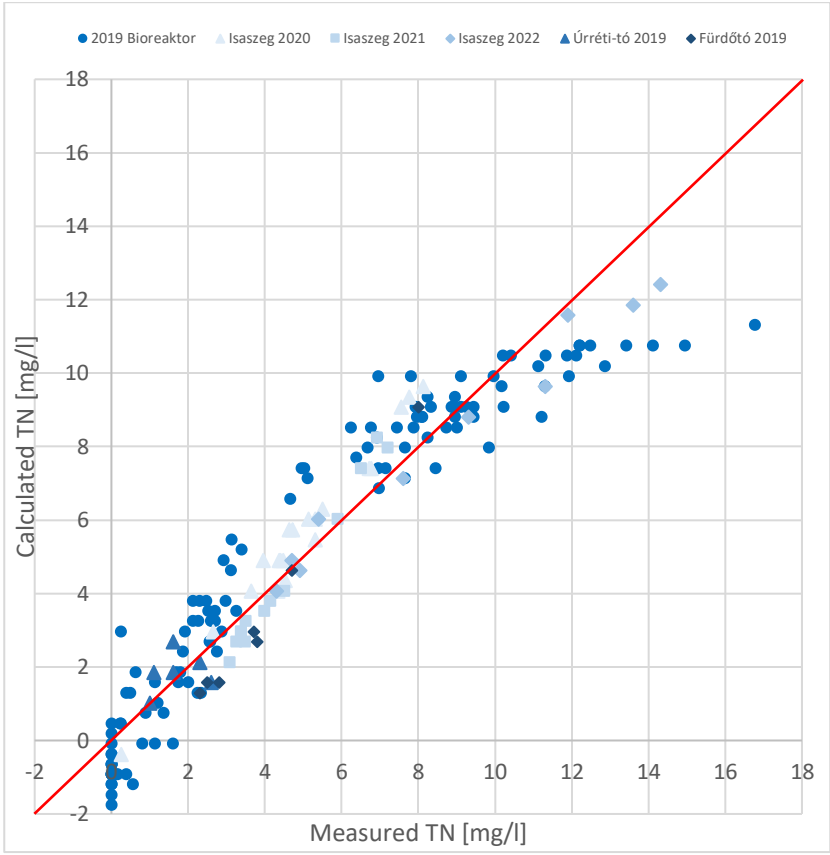

Figure 15: Plot of calculated TN values versus measured TN values and validation data.

After the error search, I found that the model RGB B band is able to determine TN concentrations based on instantaneous colour between 135 and 170 (∓ 3%), above which (TN concentration > 10mg/l) the uncertainty of the colour-based estimation increases. The B band of the RGB showed a minimum (for TN=0mg/l) value of 135 (∓ 3) during the measurements. The TN limit value is capped between 1.4 and 4 mg/l, depending on the area and watercourse, in the Decree 10/2010 (VIII.18) VM, so the procedure provides a cost-effective, instantaneous limit value-based assessment of the status of the water body, whether laboratory measurements are necessary or whether intervention is timely to improve the ecological status of the water body.

3.2. Results of the correlation study of water colour and PO_4 content

I focused on PO4, another major pollutant of our domestic and EU water surface, with the following tests. In 2020, I set up the measurement series again, again at the comparative bioreactor space at the Environmental Laboratory of the Faculty of Mechanical Engineering of Szent István University.

The measurement series started on 20.04.2020 and lasted for five months (last sampling on 18.09.2020), with three weekly sampling and measurements. The measurement was stopped 4 times and the experimental reactor was emptied and refilled with mains water. The water from the two reactors was then circulated into each other for 2 hours to obtain the most homogeneous initial condition possible. In addition to the PO_4 content and colour analysis, I also measured water temperature, pH, occasional calcium and, since I filled the basin with mains water, copper loading. There was no correlation between temperature and PO_4, or between temperature and colour, so I will use this as an interval for the rest of this series of measurements and only as an interval between new scientific results.

The results of the search for correlation between color space and PO4 values are summarized in Table 2 for both bioreactors, and the visual representation of the experimental reactor is illustrated in Figure 16.

Focusing on the G-band after the correlation search is illustrated in Figure 17 (experimental reactor) and Figure 18 (control reactor).

Table 2: Results of the correlation search between PO_4 and colour space in both experimental reactors.

	R/PO_4 corr	G/ PO_4 corr	B/ PO_4 corr	$R_{kontrol}$/ $PO_{4kontrol}$ corr	$G_{kontrol}$/ $PO_{4kontrol}$ corr	$B_{kontrol}$/ $PO_{4kontrol}$ corr
Correlation	0,17	**0,96**	-0,09	0,22	**0,87**	0,16

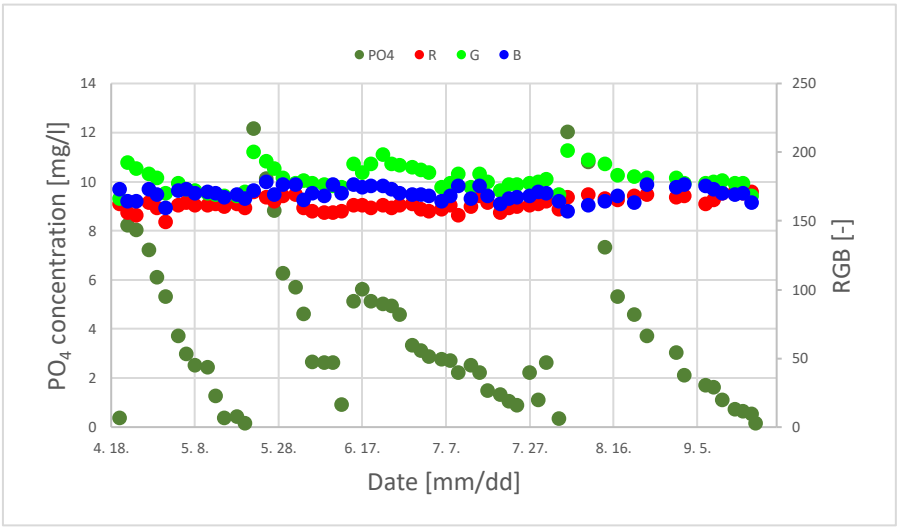

Figure 16: Measured concentration of PO_4 in the experimental reactor and measured values of the RGB colour space.

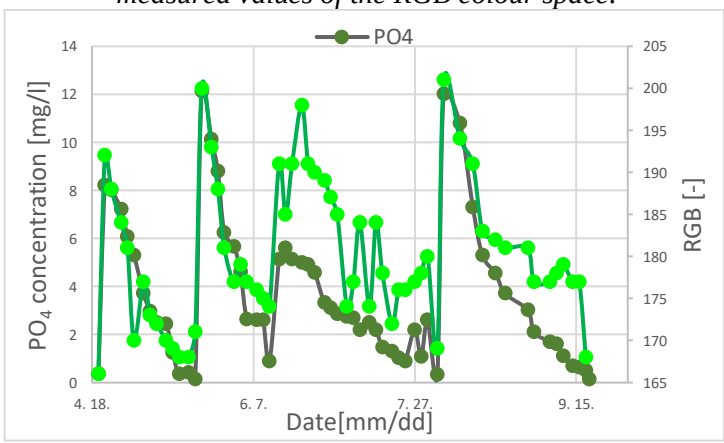

Figure 17: The measured PO_4 values of the experimental reactor and the G band of the RGB colour space.

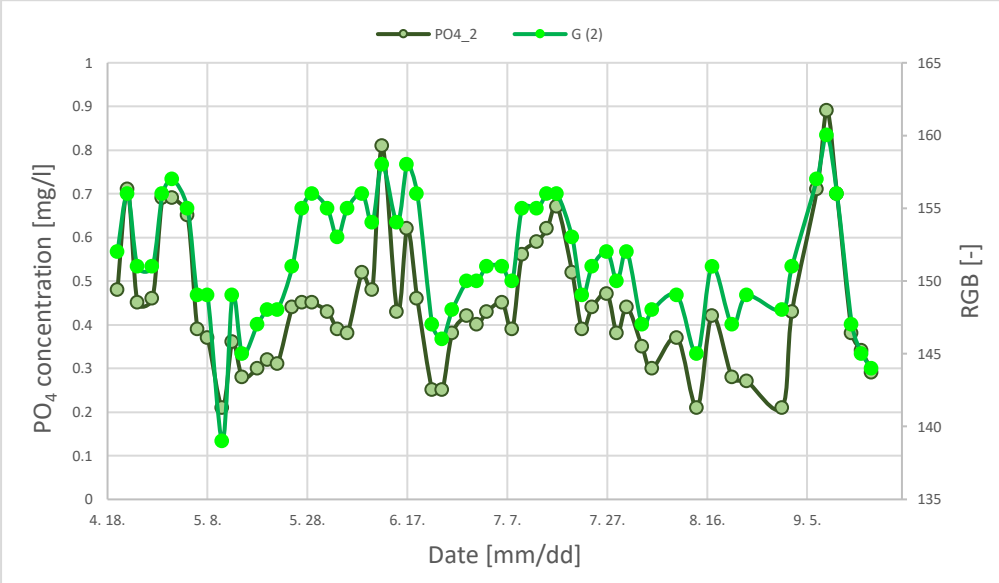

Figure 18: The measured PO_4 values of the control reactor and the G-band of the RGB colour space.

Plotting the measured PO_4 values as a function of the G-bar, after a linear line fitting, the experimental reactor R^2 is 0.92 and the control reactor R^2 is 0.75. Due to the overlap between the measured PO_4 values of the two reactors, I plotted the measured values of the two reactors in the same coordinate system, so I identified the system from 120 points instead of 60. The resulting linear line had an R^2 value of 0.87 (Figure 19).

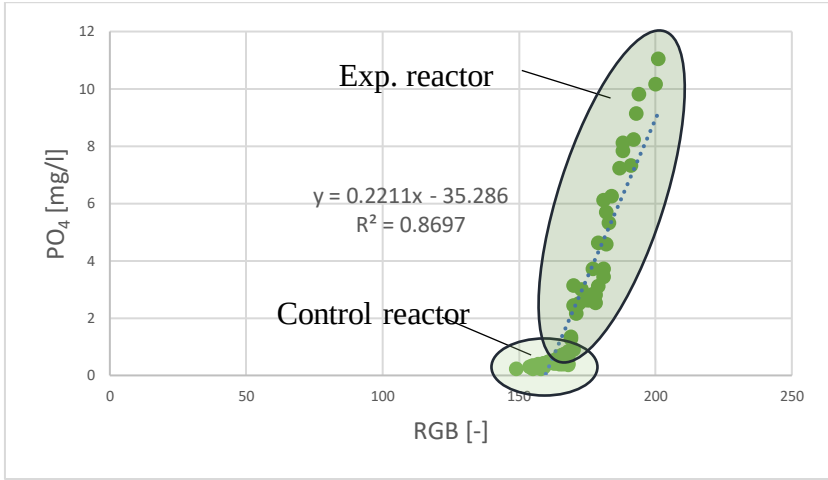

Figure 19: Plots of PO4 values as a function of the G band of the RGB colour space, with measured data from both reactors

However, the aggressive treatment of the experimental basin was not in accordance with the Decree 10/2010 (VIII.18) VM, which is much less permissive with PO_4 (or TP) values, so I performed the modelling in accordance with the Decree, but differently from 3.1. Furthermore, the scope of the regulation covered all the water bodies I measured, and the validation data were always below the limit. I split the identification values in two, creating sets below and above the limit, and identified and validated them separately. The identification of the below-limit set was carried out in a similar way as before, by plotting the PO_4 values measured in the control reactor as a function of the RGB colour space G band (Figure 20), applying linear regression, and then plotting the PO_4 values calculated from the resulting equation as a function of the measured values (Figure 21). The calculated equation is shown below:

$$PO_4 = 0{,}0312G - 4{,}2809$$

$$R^2 = 0{,}7535 \quad (4)$$

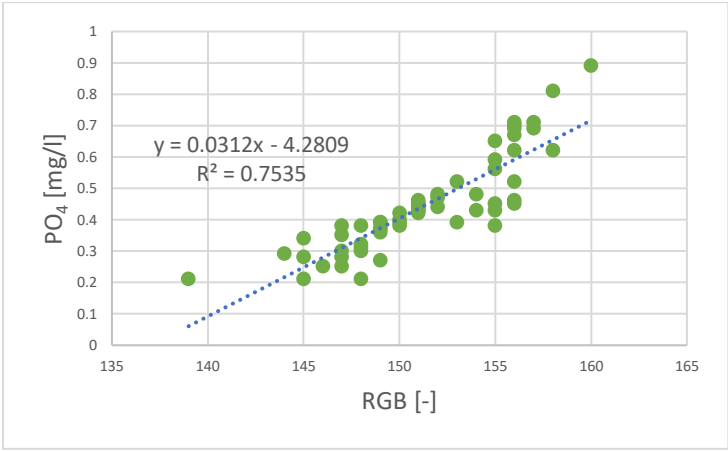

Figure 20: Plot of PO4 values measured in the control reactor versus G-band.

I then fitted the measured validation values, where I fitted the equation obtained earlier to the measured colour space values to get the calculated values. The validation data was collected from five sites, resulting in a total of 80 data points to validate the 60-member identified model. I then performed an absolute error search followed by a relative error search per measurement range. In the range $PO_4 < 1mg/l$: $h_C = 4\%$.

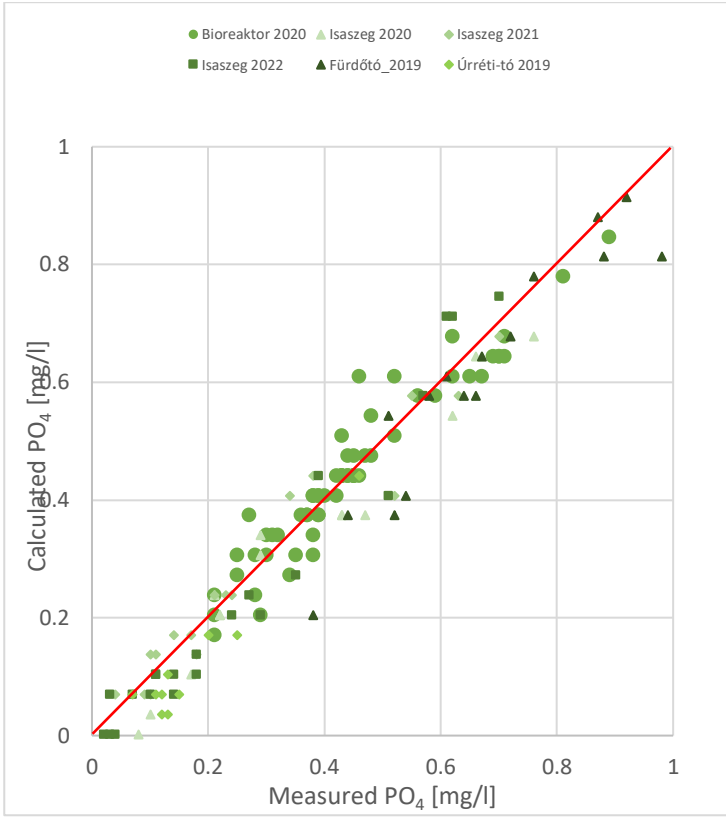

Figure 21: Plots of calculated PO4 as a function of measured PO4 values and validation data, range below 1 mg/l.

After validation and debugging, I found that the model is suitable for determining PO_4 concentrations based on instantaneous colour between RGB G band 138 and 163 ($\mp$ 2). At G > 163 ($\mp$ 2), the ecological status of the water body does not comply with the requirements of the Decree 10/2010 (VIII.18) of the VM, so laboratory measurements are necessary and possible interventions should be initiated according to the values measured there. The end of the study was in September 2020, when the area was also photographed by unmanned aerial vehicle, and the difference is clearly visible to the naked eye; the colour of the experimental bioreactor is much greener than that of the control bioreactor (Figure 22).

Figure 22: The water colour of the experimental reactor on the left is much greener (visible to the naked eye) than the water colour of the reference reactor on the right.

3.3. Colour detection of wastewater in the anoxic reactor of a wastewater treatment plant using remote sensing

In this test, I used remote sensing to determine the colour of water surfaces rather than direct colour measurement, and the measured PO_4 results are from an accredited laboratory. The study started on 22 September 2021 and was recorded 1 time per week for 12 weeks. In addition, I visited the WWTP 3 extra times, making a total of 15 measurements over the nearly 3-month measurement interval.

As it is a remote sensing technique, colour accuracy was of particular importance in the study, as the images were not recorded with a calibrated colourimeter but with a digital CMOS sensor and lens elements in front of it. The natural differences in field illumination caused by weather conditions are

mitigated by the white balance adjustment, which is both uncertain from a colour measurement point of view and less concerned with possible airborne or airborne disturbances (dust, pollen, etc.). In order to eliminate these disturbances, instead of using white balance adjustment, I performed surface reference colour measurements with the calibrated colourimeter at the edge of the anoxic reactors, using the colour average obtained there as the reference point in each case, so that the colour accuracy was as accurate as possible.

I then took to the air with the unmanned aircraft and pointed the vehicle at the GPS coordinates programmed during the first flight (first time I manually composed the maximum possible overlap, later the aircraft was programmed to fly exactly there). The altitude was 20 m, the camera was pointed at the nadir point at the separation point of the anoxic and aerobic reactors. For each shot, 3 images were taken, 30 seconds apart. After adjusting the colour accuracy, I selected the right reactor in Figure 23 as the target area in the images and averaged the pixel values using software to obtain the colour representative of the reactor. Since the reactor is under technological mixing, its contents can be considered homogeneous, so the homogenized-averaged colour is a good characterization.

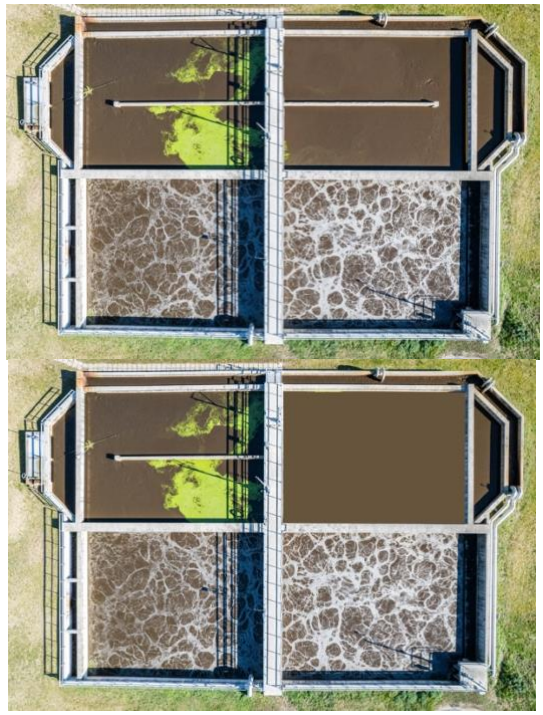

Figure 23: Photograph and averaged colour analysis of the anoxic reactor of the Gödöllő wastewater treatment plant.

The evaluation of the data started with a correlation search, the results of which are summarised in Table 3. The table illustrates that all bands in the RGB colour space shown here, unlike previous studies, are all highly correlated when I searched for correlations as a function of measured PO4 values. To shed some light on this from a different perspective, I changed the colour space and performed a correlation search in CieLAB colour coding. The reason for doing it in CieLAB colour space is that here one value (L) is the "luminance" value of the colour, and the other two values represent the resulting colour in a coordinate system. So it approaches the same colour from a completely different aspect. Table 4 shows that there is a strong correlation between the PO_4 content of the study area and the lightness of the colour of the area.

Table 3: Correlation between measured PO_4 and RGB colour space.

	R/PO_4 corr	**G/PO_4 corr**	**B/ PO_4 corr**
Correlation Value	**0,66**	**0,98**	**0,77**

Table 4: Correlations between measured PO_4 and CieLAB colour space.

	L/PO_4 corr	**A/PO_4 corr**	**B/ PO_4 corr**
Correlation Value	**0,96**	-0,71	0,42

Referring to Table 4, further analysis of this series of measurements was no longer performed in RGB colour space but in CieLAB colour space. The lightening is probably due to increased biological activity due to higher nutrient content, which could be in the form of microbubbles or even foaming. Light glancing off the surface of the bubbles may create a brighter area when it reaches the remote sensing sensor (due to the extra energy reaching the sensor), so that the sensing may show a brighter colour on average. Figure 24 shows the values of PO_4 concentration and the L band of the CieLAB colour space.

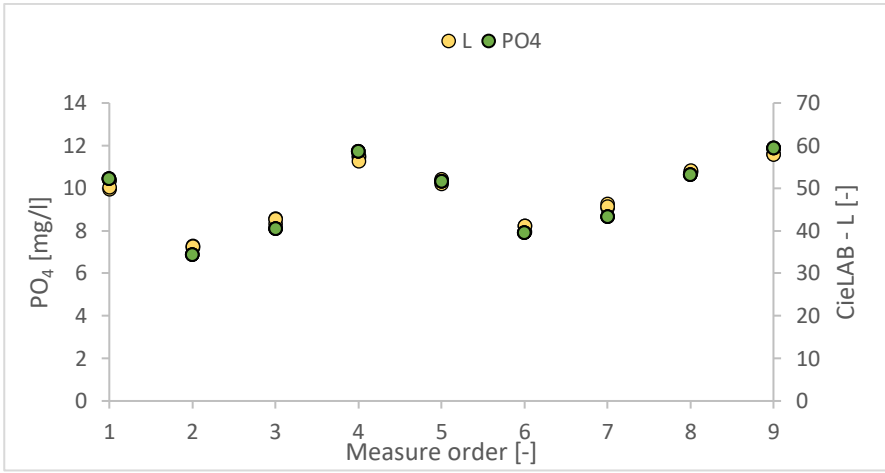

Figure 24: PO_4 and L values of the measurements.

I identified the model by measuring the first two months. For identification, I first examined the measured PO_4 values as a function of the L band of the CieLAB colour space (Figure 25). I used linear regression and obtained the following equation:

$$PO_4 = 0{,}2299L - 1{,}5509$$

$$R^2 = 0{,}981 \quad (5)$$

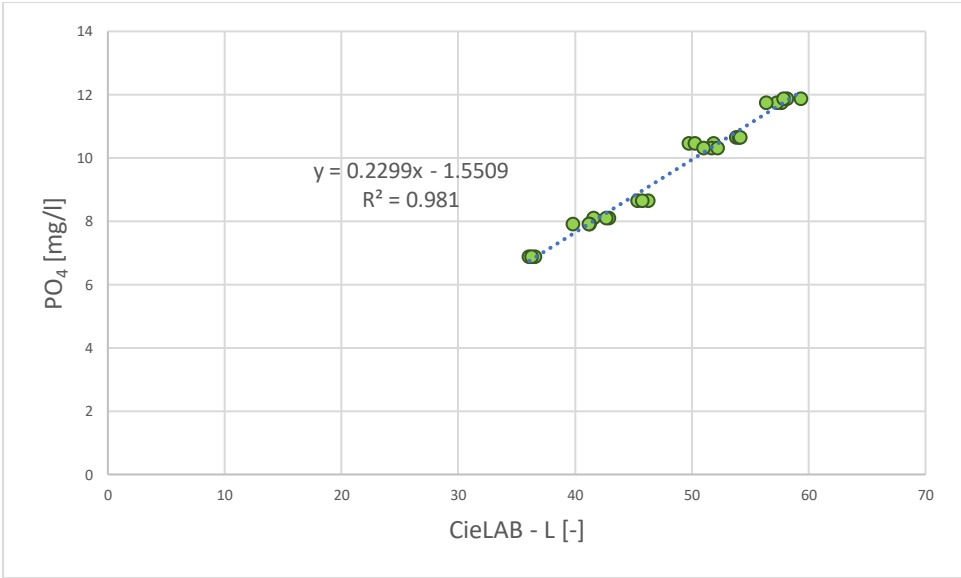

Figure 25: Plot of measured PO_4 values as a function of the L band of the CieLAB colour space.

I applied the resulting equation to the measured L values to obtain calculated PO_4 results, plotted these as a function of measured PO_4 values, then plotted the additional measured values as a validation, validation being performed on the additional six measurements (these six include the three unplanned measurements). I demonstrate this in Figure 26.

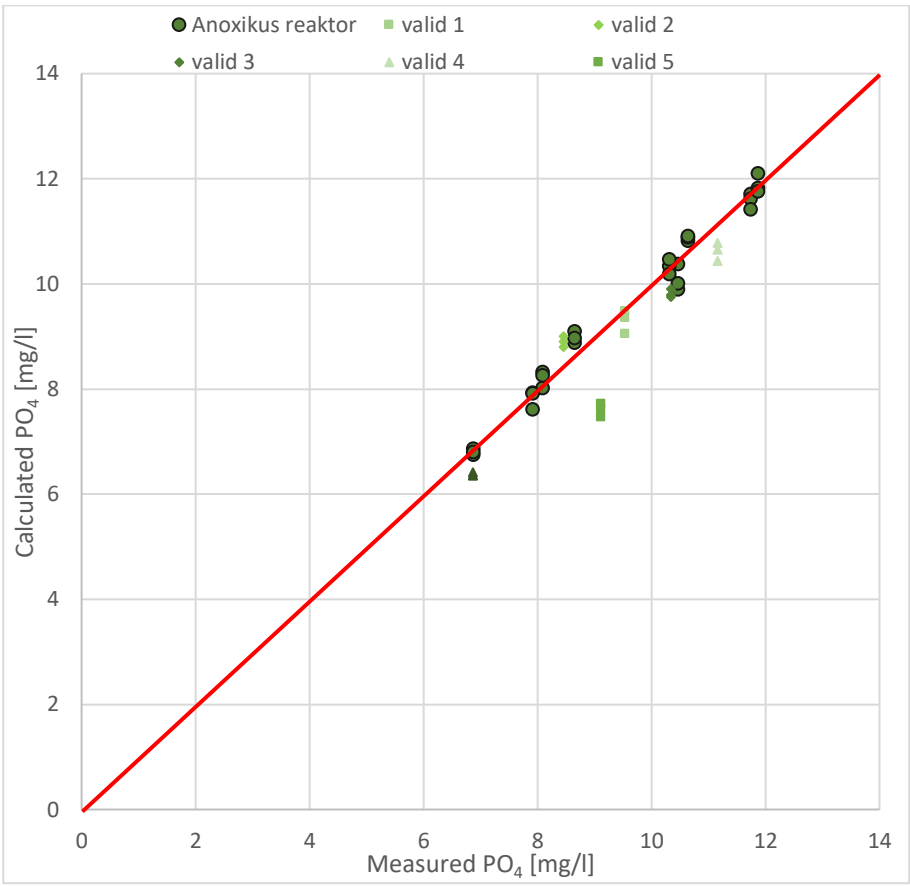

Figure 26: Plots of calculated PO_4 values versus measured PO_4 values and validation values.

Further remote sensing measurements were made impossible due to the Russian-Ukrainian conflict, which escalated into war in February 2022 and affected our country, and drone take-offs were restricted over strategic points, including wastewater treatment plants.

3.4. Uncertainty caused by waves from unmanned aircraft wings

It is an obvious phenomenon that when flying with unmanned aircraft, the air movement generated by the aircraft's rotary wings affects the area under the vehicle. Remote sensing with such devices is still in its infancy and is mainly carried out over solid areas, for example in agriculture. However, on water surfaces, the target area may react differently to drones hovering or passing over it. The aim of my study was to define and describe the impact of C1 drone-induced air motion on water surfaces.

I started the study in a bioreactor at the MATE Environmental Sciences Laboratory, which I had used previously; I installed an Ahlborn FVAD 15 type wing-wheel wind speed meter in the bioreactor above the process water level (Figure 27).

Figure 27: Photograph of the nadir taken by the DJI AIR S2 drone in the pool from a height of 2 metres.

As a function of altitude, I measured the wind speed generated by the drone in the immediate vicinity of the water body. Manual control, however, often resulted in uncertainty, so I chose programmed flight: the drone was programmed to hover at altitudes of 0.5; 1; 2; 3; 4; 5; 6; 7; 8; and 10 meters, with altitude changes at the highest possible speed, and so I measured the three main maneuvers separately: hovering (Hover), ascending (ASC-Ascending) and descending (DESC - Descending). I repeated the measurement series five times with a DJI Air S2 drone and, in order to get a more comprehensive view of the category, I repeated the measurement series five to five times per drone type in a similarly programmed manner with two other drone types (DJI Mavic Pro, DJI Mini 2).

The measured results were recorded, averaged and plotted with the standard deviation values. Figure 38 clearly shows that the most intense air movement is at low altitude and that the largest scatter is also in this range. Furthermore, Figure 58 also demonstrates that at 6 m altitude, descent (DESC) has no measurable effect and hover or climb has low values, above which there was no measurable effect on any of the unmanned C1 aircraft I flew. Thus, I have maximised my further tests for disturbance effects from rotary wing aircraft to 6 m altitude.

I also took into account possible natural winds as a source of uncertainty, and looking at the data from an installed wind speed meter only three metres from the experimental area, it can be concluded that there was no or negligible natural wind movement (below 0.2 m/s in all cases) during the measurement series, and therefore could not have affected the measured results.

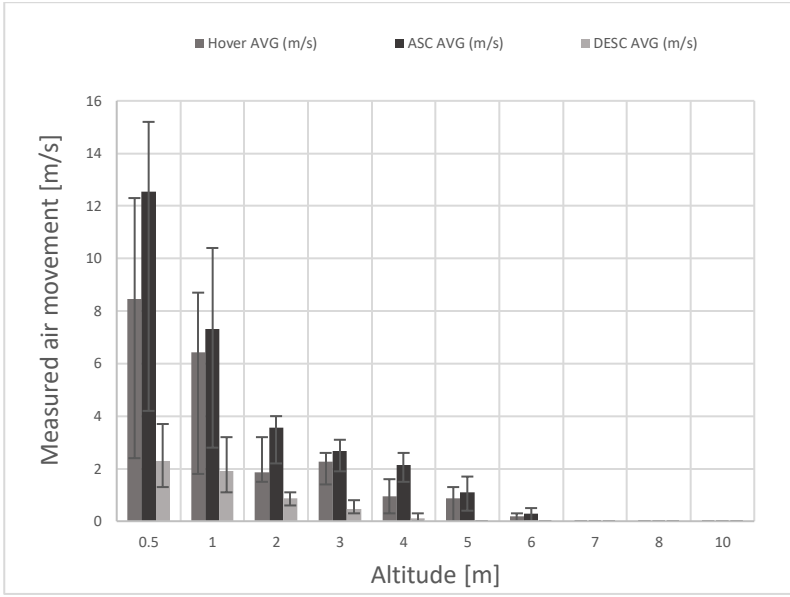

Figure 28: Representation of the air movement velocity generated by the C1 unmanned aircraft rotorcraft wings per altitude.

My next series of tests was to see how the image captured by the unmanned aircraft is affected by the air motion generated by the rotary wings when the target area is water. I repeated the measurements with my DJI Air S2 drone at three locations, seven times in total. At each site, I did not measure wind speed, but took a total of four images of the water surface below the drone at the heights I had previously measured (0.5; 1; 2; 3; 4; 5; 6 meters), averaged these images after colour correction, and compared the resulting values. The air movement generated by the rotors causes the water surface to ripple and ripple, so the flicker arriving at the sensor is also averaged. Since the flicker appears as "burned out" pixels on the sensor and "lights up" the average overall, I considered a CieLAB color space to be appropriate for this study. In order to have comparability to the resting state, I raised the drone to 2 meters and 4 meters using a ladder and a pole without rotary launching and took images of the water surface without the influence of the rotary launchers.

Figure 29 shows a focused plot of the L-value versus height; I have also shown the L-values at rest with dashed lines and the equations showing the L-value decrease. Figure 29 shows that the L band decreases with increasing height, but there is no significant difference in the slope of the lines. Furthermore, already at a height of five metres, the air motion generated by the unmanned vehicle has no detectable effect on the water surface below.

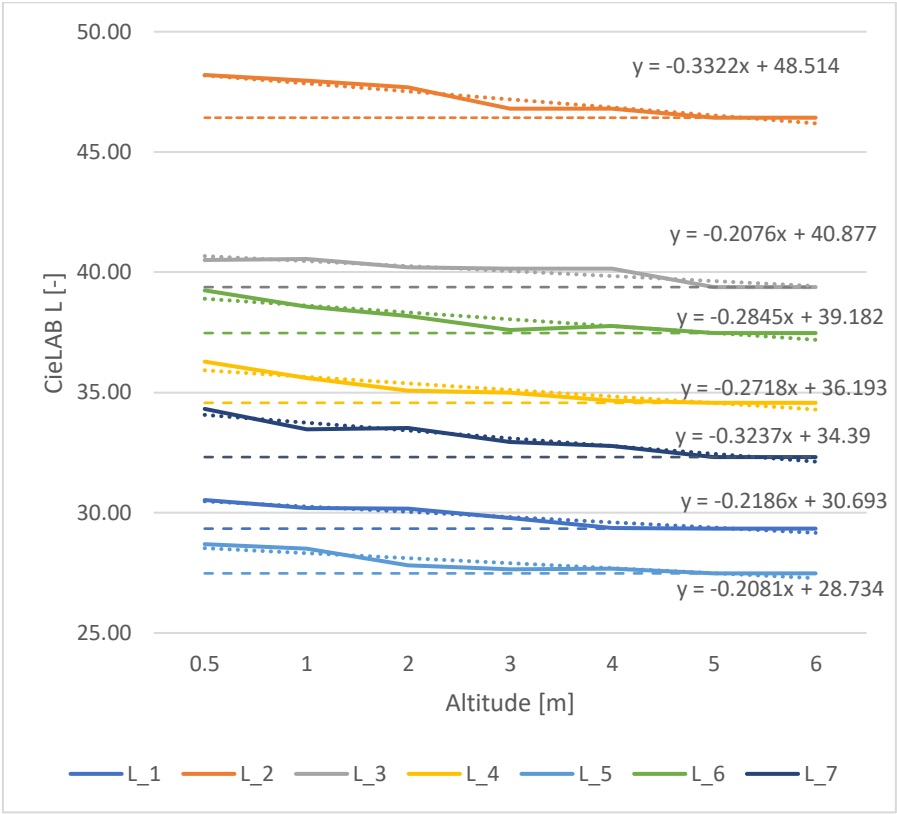

Figure 29: Plots of the CieLAB values versus altitude: the decrease of the L value, plotted with the slope of the trend lines, and the dashed line showing the resting positions.

However, when recording water below five metres, the air movement generated by the rotors increases the uncertainty in the analysis of the recorded images, which can be detected even with an 8-bit sensor. To compensate for this, I have developed a set of procedures.

The first part of the procedure is to describe the difference between the averages of the images taken at different heights and the average of the recorded water surface without the rotary wing at different heights. To do this, I plotted the L values measured during flight as a function of the rest L values, separated by altitude. Linear regression was applied, the L values calculated with the resulting formulae, and a relative error analysis over the measurement range was performed. This resulted in an altitude function with an R^2 at the time of measurement above 0.98 for all measurements, with no error deviation greater than 2% (h_{SZ} < 2%). The resulting altitude formulae are summarised in Table 10, where the resting values are given as L_{ny} and the measured values as L_m.

Table 5: Correction equations for measured values to determine the resting values as a function of height.

Altitude [m]	**Equasion of deviance**
0,5	$L_{ny} = 0{,}9794L_m - 0{,}7861$
1	$L_{ny} = 0{,}9564L_m + 0{,}6189$
2	$L_{ny} = 0{,}9703L_m + 0{,}2585$
3	$L_{ny} = 0{,}9937L_m - 0{,}1976$
4	$L_{ny} = 0{,}9801L_m + 0{,}3901$
5	$L_{ny} = L_m$
6	$L_{ny} = L_m$

Compensating the measured values with the values shown in Table 5, we obtain the resting water surface value for the CieLAB-L scale. Table 5 also shows that there is no noticeable difference at heights of five and six metres, so no compensation is needed at these heights.

The second part of the procedure is to remove the uncertainty due to the randomness of the air motion caused by the waves generated by the rotors. For the test, I set the recording to burst mode, so that I took ten images of the area within three seconds. I superimposed the images in HDR mode and tried several blending (layer blending) modes, but the blending modes only amplified the differences between the images, so the layer blending had the opposite effect to the desired one: the average colour values of the target area became increasingly distant from the colour of the resting position.

I used increasing member averaging to reduce uncertainty. Based on the already processed and averaged CieLAB-L values of the processed serial recordings, I always added one member to the averaging, looking for the value where the inclusion of a next member in the averaging no longer changes the rounded value of the average. A total of 16 serial recordings were made over bioreactors set up in the Environmental Technology Laboratory at MATE. When analysing the measurements, the scatter of the pixel mean of the recorded images was below 10% in all cases (checked in CieLAB and previously in RGB colour space). When performing ascending tag averaging on the 10 tag images of the 16 series, I found that for RGB colour space, after a maximum of six tags, the next seventh tag does not change the average, and in some cases, five tag averaging was sufficient. Since the RGB colour space is characterised by integers, I also checked it in CieLAB colour space, where the averaging was more scattered due to the resolution up to two decimal places, here no further change occurred after the eighth member.

Of course, these averaged values do not cover the true colour value of the water surface, they only reduce the uncertainty caused by the variability of the generated waves. The true value of the water colour was obtained by

performing the height formula compensation on the averaged colour value at the height at which the series images were taken. Thus, after the complex series of measurements, I found that this procedure can reduce the uncertainty caused by the airflow generated by the rotary wings of unmanned aircraft even for a fixture with a colour depth of 8 bits.

3.5. Investigation of the assumed colour perception distortion of unmanned aircraft by altitude

In subsection 3.4, I described the uncertainty caused by the air motion generated by unmanned aircraft rotor blades at altitudes below 10 m. In this subsection, I describe my measurements to detect the assumed distortion between 10 and 120 meters, and the resulting measurement uncertainty, and the evaluation of the measurements. My aim was still to investigate water surfaces.

I carried out the study over the Isaszeg nursery pond No. 4, using a programmed trajectory, on six different occasions, at 12 altitudes (10 m, 20 m, 30 m, 40 m, 50 m, 60 m, 70 m, 80 m, 90 m, 100 m, 110 m, 120 m), this 10 m altitude step is shown in Figure 61. I programmed the programmed trajectory to be as fast as possible, so that 96-100 seconds in total elapsed between the lowest and highest point being recorded, so that changes in the water were negligible. Measurements were taken with nadir point focus, repeated four times on each occasion.

I performed the evaluation of the measured data in the CieLAB colour space, because the measurements described in subsection 3.4 gave more accurate results than remote sensing with an 8-bit sensor. Furthermore, for this study I

was not looking for changes in water colour, but for possible calibration of the sensor as a function of height, so the CieLAB colour space was the most suitable for this study. In order to ensure the colour accuracy of the recordings, I took a surface measurement with a colourimeter from a concrete structure built on the south-east corner of the nursery pond, and used the colour determined here as a reference for white balance adjustment; any possible atmospheric disturbances (e.g. dust, pollen) should not affect the measurement.

The images were taken at ideal times for measurement; although cloud cover varied, there was no precipitation or significant wind. The recording time was between 10:00 am and 2:00 pm.

After adjusting the color accuracy, the target area was circled and pixel averaging was performed. Thanks to the 20 MP images, the images captured at an altitude of 120 m were sufficiently detailed to allow accurate delineation. The pixel overlay as a digital homogenisation was appropriate here because the mixing system previously installed in the lake is still in operation today, so the lake water can be considered homogeneous.

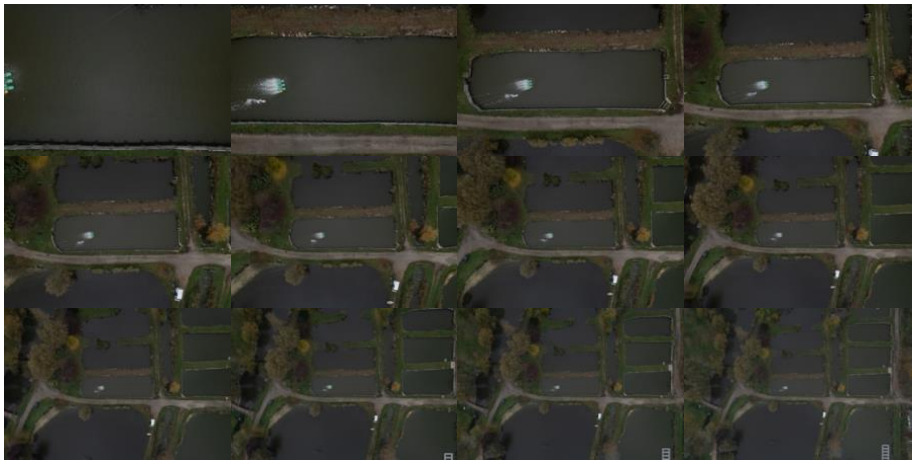

Figure 30: Drone images of nursery pond No. 4 from 10-120 m with a 10 m ascending step.

The averages were first evaluated in coordinate system, so that I could visually examine the resulting data set. However, the evaluation confirmed that the differences in height are negligible and random. Thus, I averaged the values measured at all heights (10 m - 120 m, Figure 30) per measurement, examined the variation and then performed a relative error analysis per measurement range. The mean, minimum and maximum of the error over the range are shown in Table 6 below. The negligibility of the discrepancies is also confirmed when plotted in the coordinate system, Figure 31 illustrates the AB plot of the six measurements, where A values are on the y-axis and B values are on the x-axis. While differences are visible, I have set the scaling to between -5 and 5 for visibility, but in Figure 32 I demonstrate the values of the first measurement over a real range of values (-128 to 128)

Table 6: Average, minimum and maximum values for the range of error estimates.

	L	**A**	**B**
Minimum	0,2%	0,1%	0,2%
Maximum	0,5%	0,3%	0,3%
AVG	0,3%	0,2%	0,2%

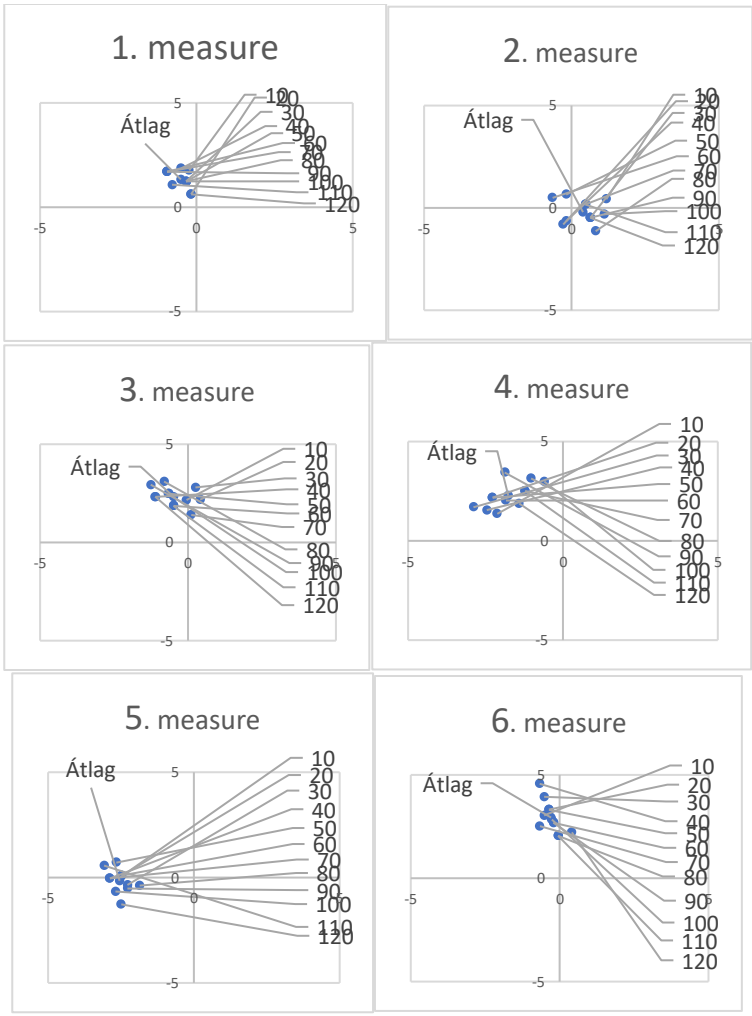

Figure 31: Plot of the values of the six measurements CieLAB - AB in the coordinate system (A=Y, B=X), in a restricted range. (Átlag=AVG)

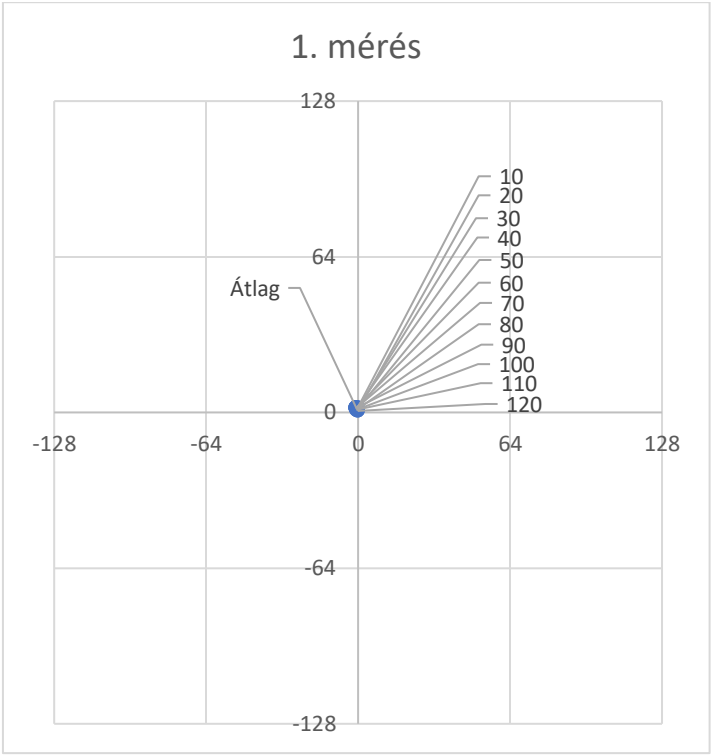

Figure 32: Values of the first measurement plotted in coordinate system, real range of values (A=Y, B=X).

The measurements show that there is no relevant or mathematically describable difference in the CieLAB colour space between the remote sensing images of unmanned aircraft with 8-bit sensors. This result may have practical benefits, as it allows a larger area to be surveyed in a single flight when surveying open water surfaces, significantly reducing the time required for the survey, and reducing the need for battery replacement and recharging in unmanned aircraft.

3.6. Testing and evaluation of image recorders with additional 8-bit CMOS sensors for colour accuracy and colour fidelity

My goal was to create a low-budget system, so I started to test several CMOS sensor devices to see how the colorimetric values at the time of color detection deviate from the values measured by a calibrated colorimeter. I first measured colour in a floodlit photo studio on colour posters, later homogeneous surfaces, and then tested water surfaces using five CMOS sensor-equipped devices with 8-bit colour depth of field (Canon 6D, iPhone SE, Xiaomi Mi8, SJCam 4000, DJI Air S2). The cameras had a focal length (focal length) of between 24 and 28 mm, so the sensor distance during image composition was not negligible. A total of 19 measurements were taken, with each camera type repeated three times. The evaluation was performed in CieLAB color space, since I was performing a calibration difference search for this series of measurements, and for this purpose LAB coding is more convenient than RGB color space.

I have plotted the evaluation in coordinate system so that I can visually examine the results. In Figure 33 I show the A=Y; B=X plots of four measurements (1,4,9,11) and visually confirm that there is variation, and the nature of the variation is similar in all cases. It can also be seen that the closest match to the reference point taken with NIX Color Pro is the Canon 6D DSLR camera and the DJI Air S2. It is also striking that the iPhone SE and the SJCam4000 are extremely close in all cases; this makes sense after a little research on the internet, as the two devices use the same type and make of sensor, the difference being in the lens elements and image processing software.

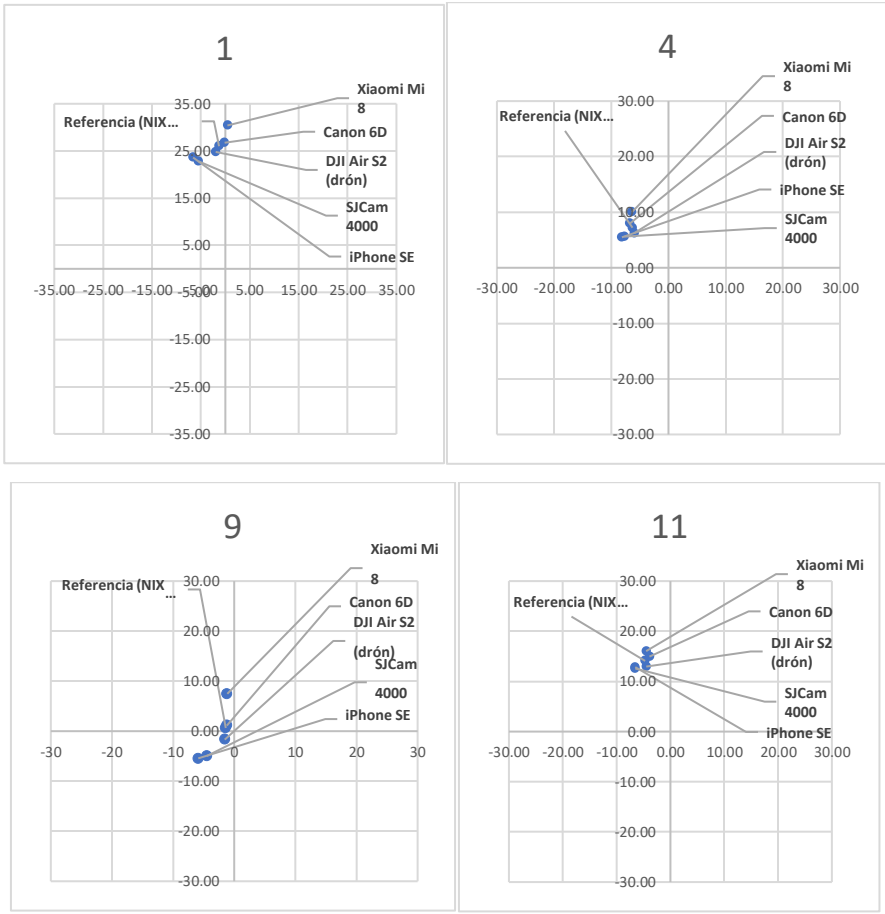

Figure 33: CieLAB - AB plot of measurements 1, 4, 9 and 11 (A=Y, B=X).

Since the deviations from the reference point are similar, I have plotted the values obtained with the image recorders as a function of the reference values. I fitted a linear line to the resulting points, and set equation expression and goodness-of-fit expression. In Figure 34, I plot the "L" bar of the Canon 6D, the "A" bar of the DJI Air S2 and the "B" bar of the iPhone SE as a function of the reference values. I used 10 of the 16 measurements for identification.

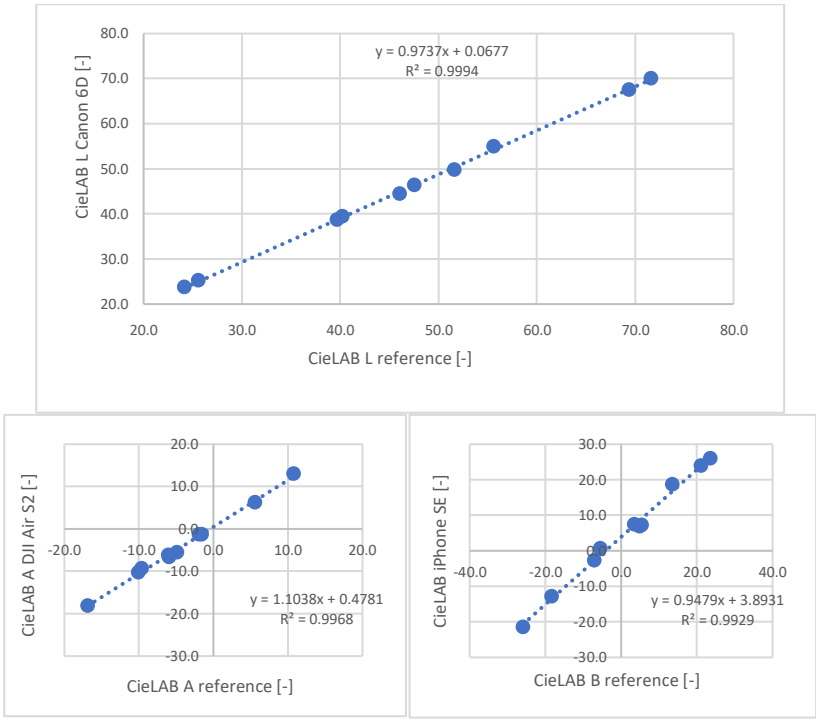

Figure 34: Some highlights of LAB values measured with image recorders as a function of reference values.

I then used the calculated equation to compute the values calculated from the measured values and plotted them as a function of each other, then added the validation values and the results of the real color measurement (reference) (Figure 35, Figure 36, Figure 37). I used this procedure to identify and validate the equation for each machine type, compensating for this to obtain an approximate value with lower uncertainty for the reference value. These equations, and the goodness of fit, are illustrated in Table 7, where the true colour value is represented by (L;A;B)v and the measured colour by (L;A;B). It can be seen from the table that the R^2 value of the fit is always above 0.97, and subsequent validation has confirmed this.

Table 7: Correction equations and R2 calculated for the devices per colour gradient (Reference: NIX Color Pro)

	L	R^2_L	A	R^2_A	B	R^2_B
Reference	$y = x$	1	$y = x$	1	$y = x$	1
Canon 6D	$L_v = 0{,}9737L_m + 0{,}0677$	0,99	$A_v = 1{,}1170A_m + 0{,}1375$	0,99	$B_v = 1{,}0198B_m - 0{,}6086$	0,99
iPhone SE	$L_v = 0{,}9744L_m + 0{,}6319$	0,99	$A_v = 1{,}1851A_m + 4{,}1743$	0,97	$B_v = 0{,}9479B_m + 3{,}8931$	0,99
Xiaomi Mi 8	$L_v = 0{,}9765L_m + 0{,}1353$	0,99	$A_v = 0{,}9533A_m - 0{,}7895$	0,98	$B_v = 1{,}0292B_m - 4{,}6895$	0,97
SJCam 4000	$L_v = 0{,}9913L_m + 0{,}1451$	0,99	$A_v = 1{,}1386A_m + 2{,}7396$	0,98	$B_v = 0{,}9447B_m + 3{,}8460$	0,98
DJI Air S2	$L_v = 1{,}0409L_m + 0{,}189$	0,99	$A_v = 1{,}1038A_m + 0{,}4781$	0,99	$B_v = 1{,}0090B_m + 1{,}3582$	0,99

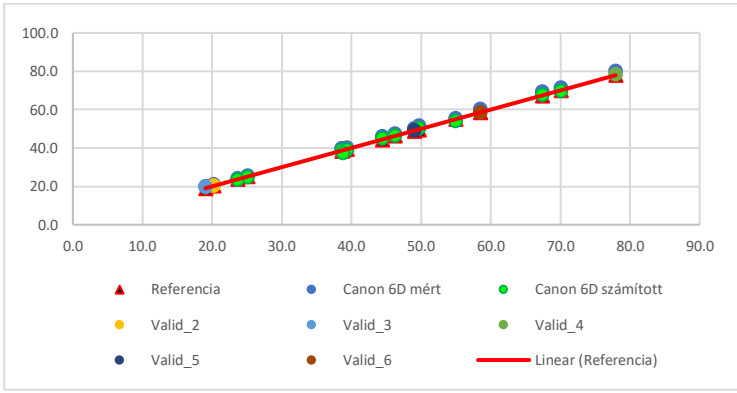

Figure 35: The measured CieLAB "L" values as a function of the calculated CieLAB values for the Canon 6D camera type and the validation values.

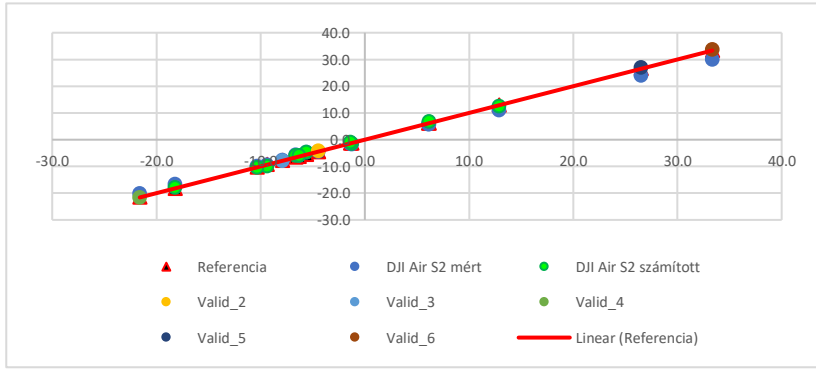

Figure 36: Measured CieLAB "A" values versus calculated CieLAB values for the DJI Air S2 machine type and validation values.

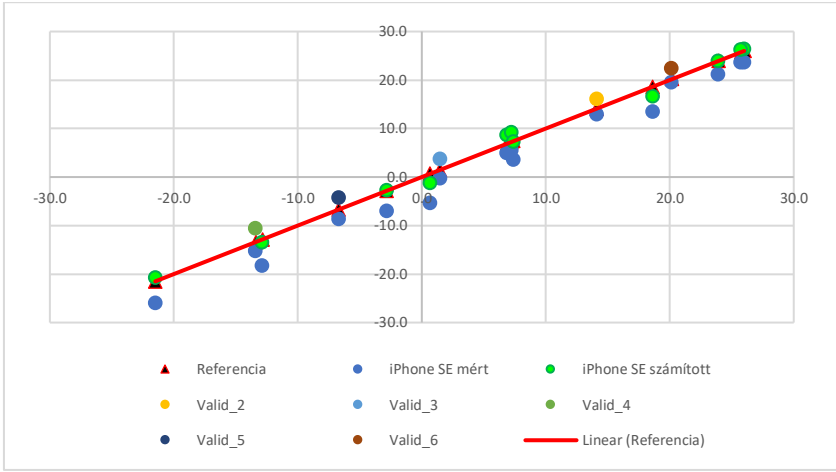

Figure 37: Measured CieLAB "B" values as a function of calculated CieLAB values for the DJI Air S2 machine type and validation values.

Figure 35, Figure 36 and Figure 37 show that applying the calculated compensation values to the measured values gives a much stronger approximation. Thus, with the compensation values, a low computational demand post-calibration black box model can be developed, which can be applied to image sensors with CMOS sensors already at 8-bit sensitivity.

4. Conclusions and proposals

There is no doubt that in-situ or ex-situ colour measurement procedures cannot always replace in-situ or ex-situ laboratory measurements because of their accuracy, especially for 8-bit sensors.

It is important to develop more practical and/or accurate mathematical models to describe total nitrogen or phosphate ion concentrations in the context of determining good ecological status of living waters.

In my thesis, I performed a comparative study in aggressively treated and untreated bioreactors and validated it with real living water data to develop a low-computationally demanding and easy-to-use model that can be used to estimate the instantaneous ecological status of water bodies.

Furthermore, I investigated the factors that I hypothesized to cause uncertainty in the colour measurement aspect of low-altitude remote sensing by unmanned aerial vehicles for 8-bit sensors, and I investigated the colour divergence of devices with 8-bit sensors. Both studies were carried out with the largest number of devices available to me.

4.1. Estimation of total nitrogen concentrations in water

The correlation between water body colour and total nitrogen concentration discovered during the ex-situ colour assessment of water bodies was validated by validation, and the relative error over the range of values was also found to be low. However, there is no doubt that the model I have developed and presented and applied in this thesis is primarily an estimator in its current state,

which can provide guidance to pond farmers, for example, on the ecological status of water in terms of its quality, whether it is of adequate quality (low concentration), moderately adequate quality (concentration around the limit), or inadequate quality (concentration above the limit).

The use of the model does not supersede the laboratory measurements that have a larger biological footprint, but becomes necessary when the assessment of the status of a water body indicates a problem. This low computational demand and easy-to-use system can reduce the cost of water maintenance, which can be significant not only in our country and the EU, but also in areas where water status determination is partially or not done at all due to lack of access to measurements or differences in knowledge, and can help to identify potential water use and the intervention that could be required, be it in a lake, river or even in an open area wetland type of wastewater treatment.

However, a refinement of the procedure by extension is definitely needed in the future, as the colour of the water can be affected by chemical components that were not present in the bioreactors I studied and in the water bodies used for validation, so that a good chemical status of the water body can only be partially estimated by the current form of the procedure.

Furthermore, it is worthwhile to test separately not only for total nitrogen but also for nitrite and nitrate compounds, which are determinants of ecological status, thus providing an aid in the area where the load is assumed to be of sewage technology origin.

In addition, the analysis should be extended to include not only ex-situ but also in-situ measurements, such as remote sensing, low-altitude remote sensing techniques, which can be used to analyse the status of larger water bodies in detail, either as a whole or through grid network assessment.

The idea of water monitoring by image analysis was first conceived in the early 2000s in a joint project between NIKON and SEALIFE, using NIKON Coolpix 885 and SeaLife Ecoshot cameras to monitor changes in water quality by analysing a series of 2000 timelapse images (Goddijn-Murphy et al., 2009). However, the system was not capable of providing a snapshot value. Tavakoli and Gebbers (2019) measured nitrogen content using RGB analysis, but not on water surfaces but on crops, so the use of colorimetry could extend the applicability.

4.2. Estimation of phosphate ion concentrations in water

Phosphate ion is a key compound in eutrophication, so its measurement is essential to understand the ecological status of a water body. The advantages and shortcomings described in Section 3.1 apply here too; good approximations can be estimated with the model for adequate (below limit concentration), moderately adequate (near limit concentration), and inadequate (above limit concentration), but the accuracy of the model is not a substitute for ex-situ laboratory measurements, especially for concentrations above limit.

The estimation generated by the model can be used to provide information to pond owners, and as the model is simple to use and low computationally demanding, it can help pond owners in areas or wetland-type treatment plants where obtaining information may be a daily challenge.

It would also be useful to extend this study and model to low-altitude remote sensing and to investigate the relationship between water level and the phosphate ion/nitrogen form balance.

An RGB-based measurement was carried out by Godjin and White (2006), analysing the water quality of Galway Bay (Ireland) using digital technology at the time. This study was less successful due to the technological limitations of the time, with the current prevalent 8-bit colour depth capable of much more accurate imaging than the 4-bit colour depth imaging of the time. Furthermore, the study focused on salinity and chlorophyll content, rather than on the ecological stressors that are now known to cause algal blooms.

4.3. Estimation of phosphate ion concentrations in anoxic wastewater reactors

Phosphate ion content measured in anoxic bioreactors in wastewater treatment plants and the perception of water clarity (CieLAB color space, L band) are strongly correlated, as suggested by the validated model; in addition to the strong correlation, the relative error over the measurement range was low.

The method can provide a solution in areas where wastewater treatment is taking place but where, due to availability, it is not possible to use probes or to properly operate and maintain the probes used. The method is of course less accurate than a calibrated set of measuring instruments, but in many cases an estimator accuracy can result in a much better wastewater treatment than the current, mostly ad-hoc estimation. In this case, of course, an unmanned aerial vehicle would not be the ideal solution, but an affordable image recorder with at least 8-bit colour depth and low computational demand for post-calibrated value compensation can provide a good approximation of the instantaneous water status, thus making the wastewater technology tunable.

In order to make the model applicable, it is worthwhile to extend the study areas to several types of wastewater treatment processes (intensified sludge systems, wetland, MBBR, FCR) and to extend the measurement range.

Furthermore, I only have a hypothetical answer as to why higher phosphate ion content causes a change in water clarity, biological and chemical oxygen demand testing and controlled ex-situ laboratory measurements could be used to substantiate why this change occurs.

The colour of wastewater has already been investigated by Damirchi et al (2019), comparing spectrophotometer and digital camera measurements, but not for ecological contaminants, but for a form of triarylmethane, the dye compound "brilliant green" ($C_{27}H_{33}N_{2}.HO_4S$). Santiago and Seville (2022) continued their analysis of wastewater for dimethyl sulphide (C_2H_6S) using digital image capture.

4.4. Estimation of uncertainty due to air motion generated by unmanned aircraft rotor blades

In this series of measurements, I first investigated whether the rotary wings of unmanned aircraft have an effect on the water surface below, in the case of 8-bit sensor detection/colour measurement, and if so, to what extent per height, and whether this can be compensated for by some low-computational demand model.

The model can be used to compensate for water surface measurements below 6 m, as I have shown the disturbance by testing. The practical usefulness of this comes to the fore when a water surface that is more difficult to access or

covered by some kind of structure needs to be investigated and it is not possible to measure from higher up.

The model was run with three different unmanned aircraft of the same category, giving a comprehensive picture of the impact. However, it may be advisable to extend the study to several models in order to have a more accurate understanding of the uncertainty caused by the rotating wings. On the other hand, a precise knowledge of the components of the unmanned aerial vehicle, the power of the engines and the speed they generate could provide additional information, which, together with the knowledge of the mass of the drone, could improve the accuracy of the model extension.

Furthermore, remote sensing at such altitudes should be extended and combined with the studies described in sections 3.1, 3.2 to allow for an appropriate ecological assessment to be carried out in-situ.

Although the presumed negative environmental impact of drone propellers has been the subject of a number of studies, the focus has been primarily on the noise impact of the rotary blades and the resulting increase in observer impact. Liu et al (2023) compared the aerodynamic performance of rotary wings, and McKay et al (2021) described the noise impact of counter-rotating propellers, but the impact of air movement on the environment (including the water surface) has not yet been investigated.

4.5. Estimation of the uncertainty assumed by the altitude of unmanned aircraft

I have demonstrated with a series of measurements that when recording images of unmanned aircraft during a 10-120 m flight, the colour difference

is negligible when post-calibrating the colour of the recorded image to the colour of surface measurements.

The practical benefit of this result is that, for example, for a lake system, a small number of images taken from 120 m altitude is sufficient to obtain a comprehensive understanding of the current ecological state of the lake system. With fewer flights, the biological footprint of the survey is smaller, and the survey requires less battery charging if there are no difficult to access or covered parts of the lake system (in which case the procedure and model developed in 3.4 should be used).

It would be advisable to extend the procedure to several types of drones and to investigate the accuracy of the programmed flight, how far the composition of the captured images differs and how far this may cause colour differences in the surveyed areas, for example in the case of image recognition software.

It would also be worthwhile to extend the study to larger areas of water (e.g. Lake Venice or Lake Balaton) to see how naturally occurring ripples affect colour perception, similar to the need for compensation as described in Section 3.4. Of course, the flight safety of unmanned aircraft may vary from type to type, depending on wind speed. In addition to these, it would be worthwhile to conduct a comparative study on the usability of polar filters and to investigate other angles of incidence in addition to the nadir point test.

By using surface reference color measurements, I could eliminate the claims of Schamberger et al. (2022) or Wang et al. (2017) that dust or atmospheric aerosols can affect the measurement, so that the uncertainty of their observing system could be further reduced by the procedure I describe.

By using surface reference color measurements, I could reduce the effect of dust or atmospheric aerosols on the remote sensing, so the uncertainty in the measurements of Schamberger et al. (2022) or Wang et al. (2017) can be further reduced by the procedure I describe.

4.6. Investigation of additional image capture devices with 8-bit CMOS sensor, investigation of the possibility of colour measurement

The colour accuracy of digital imaging can vary from one imaging device to another, and I have demonstrated this by measuring and testing a large number of devices across a wide technological spectrum, and by creating a black box model to compensate for the differences; the colour difference depends not only on the sensor design, but also on the lens elements that shape the light and the software that processes the information, which are often unknown, as they are not always calibrated for accuracy, but to enhance the user experience.

Monitoring with available devices is present in several fields, for example Aburghin et al (2022) applied monitoring with smart devices for medical purposes, Chianucci et al (2021) performed a canopy analysis, Tuaño et al (2021) performed an analysis of the apparent amylose content of milled rice, but no comparative study on the variation of the recording devices was performed. An extension of the black box modelling procedure I have described could also make these measurements more accurate, as the need for monitoring the use of digital recorders is increasing year by year.

From a water monitoring perspective, the practical utility of this study can be linked to the results of all my previous measurements. When assessing the ecological status of water by remote sensing using colour (3.1, 3.2), monitoring any reactor in a wastewater treatment plant (3.3), or using unmanned aerial vehicles (3.4, 3.5), uncertain colour results can be obtained, but using the model can reduce the uncertainty in the area of interest.

However, it may be necessary to extend the study to the specific instruments in order to use accurate post-calibration values when performing colour assessment. Although this is not costly to assess, availability and potential willingness to do so may be highly subjective. Furthermore, we currently have no knowledge of the extent to which physical effects of use (lens scratches, possible sensor oxidation, etc.) may affect the colour of the image, so a post-calibration survey may be worthwhile from time to time.

5. New scientific achievements

1. I find that the TN (total nitrogen) content of living water bodies is strongly correlated - corr(TN,RGB_B)=0.87 - with the blue band B of the RGB colour space, TN: 0-10 mg/l, over a temperature range of 10-22 degrees Celsius, which can be described by the equation:

$$TN = 0{,}2823B - 38{,}794 \qquad (R^2 = 0{,}8755), \tag{6}$$

where:

- TN - the total nitrogen concentration,
- B - blue band of the RGB colour space

The method can provide a cost-effective threshold-based assessment, predict ecological status, determine the need for intervention, and sound the alarm.

2. I find that the PO_4 content of living water bodies is strongly correlated - corr(PO_4,RGB_G) =0.86 - with the green band G of the RGB colour space for PO_4: < 1 mg/l over a temperature range of 10-22 degrees Celsius, which can be described by the following equation:

$$PO_4 = 0{,}0312G - 4{,}2809 \qquad (R^2 = 0{,}7535), \tag{7}$$

where:

- PO_4 - is the phosphate ion concentration,
- G - the green band of the RGB colour space

3. I find that the PO_4 content of anoxic wastewater reactors is strongly correlated - corr(PO_4, CieLABL)=0.96 - with the L, or lightness band of the CieLAB color space, within the range PO_4: 6.86-11.87mg/l, over a temperature range of 12-18 degrees Celsius, which can be described by the equation:

$$PO_4 = 0{,}2154L - 0{,}6767 \qquad (R^2 = 0{,}9215), \tag{8}$$

- PO_4 - is the phosphate ion concentration,
- L is the CieLAB brightness value

4. Using a complex experimental procedure, I have demonstrated that the air motion generated by C1 unmanned aircraft wings has an effect on the water surface only below 6 m flight altitude, which influences the imaging results and increases the uncertainty significantly even with an 8-bit per band sensor. I find that for RGB colour space, this uncertainty can be reduced by further averaging the pixel averages of several images, up to a maximum of six, captured within three seconds.

5. I have experimentally demonstrated that using a reference measurement on the surface with a corrected colour balance, using low-altitude remote sensing between 10 and 120 m using a nadir CMOS sensor with 8-bit colour depth per band, there is a maximum 1% variation in the perceived colour of the water-covered target area.

The reference measurement at the surface eliminates the atmospheric composition from interfering with imaging. During the experiment, the surface reference measurement was performed with a calibrated colorimeter and the remote sensing was performed with a C1 unmanned aerial vehicle.

6. I have demonstrated through complex studies that the image processing process of digital CMOS-type image capture devices with 8-bit sensitivity per band sensor can vary in colour fidelity. Using a colorimetric tool, the discrepancy between the real and measured color bands was described and correction models were developed. The correction model can be described by a linear equation, where the slope and the axis intercept are machine type dependent.

With this post-calibration procedure, my method for water quality determination can be extended to additional digital CMOS-type imaging devices with 8-bit color depth per band sensor.

	L	**R^2_L**	**A**	**R^2_A**	**B**	**R^2_B**
Reference	$y = x$	1	$y = x$	1	$y = x$	1
Canon 6D	$L_v = 0{,}9737L_m + 0{,}0677$	0,99	$A_v = 1{,}1170A_m + 0{,}1375$	0,99	$B_v = 1{,}0198B_m - 0{,}6086$	0,99
iPhone SE	$L_v = 0{,}9744L_m + 0{,}6319$	0,99	$A_v = 1{,}1851A_m + 4{,}1743$	0,97	$B_v = 0{,}9479B_m + 3{,}8931$	0,99
Xiaomi Mi 8	$L_v = 0{,}9765L_m + 0{,}1353$	0,99	$A_v = 0{,}9533A_m - 0{,}7895$	0,98	$B_v = 1{,}0292B_m - 4{,}6895$	0,97
SJCam 4000	$L_v = 0{,}9913L_m + 0{,}1451$	0,99	$A_v = 1{,}1386A_m + 2{,}7396$	0,98	$B_v = 0{,}9447B_m + 3{,}8460$	0,98
DJI Air S2	$L_v = 1{,}0409L_m + 0{,}189$	0,99	$A_v = 1{,}1038A_m + 0{,}4781$	0,99	$B_v = 1{,}0090B_m + 1{,}3582$	0,99

6. Relevant publications related to the thesis

MTMT: https://m2.mtmt.hu/api/author/10064810

Proofread article in a foreign language:

Házi, J. ; Penksza, K. ; Barczi, A. ✉ ; Szentes, S. ; Pápay, G - Effects of Long-Term Mowing on Biomass Composition in Pannonian Dry Grasslands, AGRONOMY (BASEL) 12 : 5 Paper: 1107 (2022) - Q1; IF: 3,949

András Barczi, Gábor Géczi - Phosphorus contamination tracking via colour analyzation on algae in experimental reactors, ENVIRONMENTAL MONITORING AND ASSESSMENT - Under review - Q2; IF 3,307

Barczi, András ; Szabó, Dorottya ; Magyari, Péter ; Géczi, Gábor; Colour analysing of IPA brewing phases, including daily measuring of the fermentation process, SCIENCE TECHNOLOGY AND INNOVATION 15 : 1 , 7 p. (2022)

András, Barczi ; Gábor, Géczi - Harvesting during the process; agriculture in developed wastewater treatment plants, HUNGARIAN AGRICULTURAL RESEARCH: ENVIRONMENTAL MANAGEMENT LAND USE BIODIVERSITY 27 : 4 pp. 8-10. , 3 p. (2018)

András, Barczi - Examination of propeller gained distracting air motion in the case of remote sensing lakes and fishing ponds with C1 type UAVs, HUNGARIAN AGRICULTURAL RESEARCH

Proofread article in Hungarian:

Barczi, A.; Major, N. - Fényszennyezési esemény vizsgálata Budapest XIII. kerületében JOURNAL OF CENTRAL EUROPEAN GREEN INNOVATION 10 : (1) pp. 99-110., 12 p. (2022)

Conference publication in foreign languages:

Barczi, A ; Géczi, Gábor - Forwarding the wastewater treatment - treatment and the society, In: Farkas, István (szerk.) 23rd workshop on energy and environment: Book of abstracts, Gödöllő, Magyarország : Szent István University (2017) 32 p. pp. 21-21. , 1 p.

In: Anna, Pasternakiewicz; Michał, Miłek (szerk.) Risk Factors of Food Chain: XXIst International Conference: Book of abstract, Iwonicz, Lengyelország : Uniwersytet Rzeszowski (2021) p. 12 , 1 p.

Barczi, András ; Géczi, Gábor - Előretekintés a szennyvíztisztításban - Kezelés és társadalom, In: Lázár, István (szerk.) Környezet és energia : Hatékony termelés, tudatos felhasználás, Debrecen, Magyarország : MTA DAB Földtudományi Szakbizottság (2018) 281 p. pp. 253-256. , 4 p.

Barczi, A. ; Géczi, G. - Wastewater and harvesting: Agriculture in developped wastewater treatment plants, In: Géczi, Gábor; Korzenszky, Péter (szerk.) Researched Risk Factors of Food Chain, Gödöllő, Magyarország : Szent István Egyetemi Kiadó (2018) pp. 77-82. , 6 p.

Barczi, A. ; Géczi, G. - Wastewater and harvesting: agriculture in developped wastewater treatment plants, In: Víg, Piroska; Máthé, László (szerk.) XIX. International Conference Risk Factors of Food Chain 2018 : Book of Abstracts, Gödöllő, Magyarország : Szent István Egyetem Egyetemi Kiadó (2018) p. 15

A., Barczi ; J., Patko ; V., Nagy ; A., Barczi - Color-measurement differences during the drying of soil layers,In: Magó, László; Kurják, Zoltán (szerk.) SYNERGY - Engineering, Agriculture and Green Industry Innovation : ABSTRACTS,. Gödöllő, Magyarország : Szent István Egyetem Gépészmérnöki Kar (2019) 96 p. pp. 34-34. , 1 p.

Barczi, A. ; Géczi, G - Wastewater as potentional renewable energy source, In: Gábor, Géczi; Richárd, Kicsiny; László, Székely Efficiency, solar and thermal energy for the human comfort : Book of Abstracts, Gödöllő, Magyarország : Hungarian University of Agriculture and Life Science (2021) 47 p. pp. 45-46. , 2 p.